A novel approach to Segmentation and Registration of Echo-cardiographic Images

Thesis submitted in partial fulfillment
of the requirements for the degree of

Master of Science (by Research)
in
Computer Science

by

G.Vidhyadhari
200402045
vidhyadhari@research.iiit.ac.in

International Institute of Information Technology
Hyderabad, INDIA

February 2014

INTERNATIONAL INSTITUTE OF INFORMATION TECHNOLOGY
Hyderabad, India

CERTIFICATE

It is certified that the work contained in this thesis, titled **A novel approach to Segmentation and Registration of Echo-cardiographic Images** by Miss. **Vidhyadhari.G**, has been carried out under our supervision and is not submitted elsewhere for a degree.

Date

Prof. Jayanthi Sivasamy,
Professor,
IIIT, Hyderabad

To my Family.

Acknowledgements

I would like to thank my guide, Dr. Jayanthi Sivaswamy, for her support and guidance during my research over the past few years. She has given me freedom to explore different research topics, the experience which I can cherish in my lifetime. Her sincerity and critical perception has made me learn many things. I am thankful that I have got an opportunity to work under her guidance.

I am grateful to all the people who gave their time and valuable suggestions during my thesis. I thank my labmates Gopal, Sandeep, Subbu, Sai Deepak, Harini and Kartheek for their valuable comments which made my piece of work better. I am also thankful to my friends - Sheetal, Priyanka, Mrityunjay, Dileep - for making the time spent in lab memorable and supporting me. I would also like to thank my friends Haritha and Poornima who have made stay at IIIT wonderful,

Above all, I am thankful to my family for their patience and support. I am thankful to all those who have helped me at some point or other and my research center CVIT where I have first learnt about research.

February 8, 2014

Abstract

Echo-cardiographic images provide a wealth of information about the heart(size, shape, blood flow rate, etc) and are therefore used to assess the functioning of heart. Automated analysis of echo-cardiographic images are aimed at extracting a displacement field which represents the heart motion. Such a field is critical for extracting higher order information which is needed for diagnosis of heart diseases. However, these images are very noisy which poses a huge challenge to image analysis.

Most of the methods used for the analysis of the echo-cardiographic images are designed in such a way that they are very specific to the noise present in the echo-cardiographic images. These methods can be categorized into two categories: (i) de-noise the signal prior to analysis and (ii) formulate input as a noisy signal to model the noise using statistical noise model. In this thesis we propose algorithms for analysis of echo-cardiographic images which do not require any pre-processing step or explicit handling of noise present in the images.

We present novel algorithms for segmentation and registration of echo-cardiographic images in this thesis. These two algorithms are designed based upon noise-robust image representation. This image representation is obtained by computing a local feature descriptor at every pixel location. The feature descriptor is derived using the Radon-Transform to effectively characterise local image context. The advantage of this representation is that, in addition to being robust to noise, it provides a good detail of the distribution of the pixel intensities in the image. Next, an unsupervised clustering is performed in the feature space to segment regions in the image. This feature-space representation is also used to extract hierarchical information for image registration.

The performance of the proposed methods is tested on both synthetic and real images. A comparison against well established feature descriptors is carried out to demonstrate the strengths and applicability of the proposed representation. Overall, the results indicate promise in the strategy of doing segmentation of noisy data in image.

In this thesis, the algorithms are designed in such a way that the algorithm works efficiently even in presence of high level of speckle noise and doesn't require any pre-processing. Moreover it can be easily adapted to any other modality. The main contributions of this thesis are:

1. Noise-robust representation of an image in feature space.
2. Segmentation of an image using feature space
3. Registration of images using hierarchical information.

Contents

List of Figures

List of Tables

Chapter 1

Introduction

1.1 Introduction

Medical imaging techniques are used to acquire images of the structural and functional aspects of the human body. These images are acquired to capture specific information of the body using various modalities, unlike natural images, which usually contain all the information visible in the optical range. Since the internal aspects of the body are not directly visible, it is often approximated based on the physical properties on the imaging modality used and the body part being scanned. Therefore, the application of physical principles in the design and development of medical imaging modalities and medical images are much more varied and complex than general photography. Some modalities popularly used in medical imaging are as follows: (a) Optical Imaging (b) Ultrasound (c) Computed Tomography (d) Magnetic Resonance Imaging etc. Only optical imaging is based on the usage of light in the visible range, others use x-ray, magnetic field, sound signals and nuclear radiation etc. Due to the complex acquisition process, the images are noisy and have low contrast. One such medical imaging technique of interest in this thesis is Echo-cardiography.

Echo-Cardiography is used to diagnose cardio-vascular diseases [1]. It is a sonogram of the heart. The image of the heart is taken using sound waves. It is obtained as a video which has images of heart at different stages of contraction and relaxation. It provides wealth of information like the shape and size of the heart, velocity of blood flow and the location and extent of the damaged issues present. Due to its non-invasive and inexpensive nature, it is one of the most primary diagnostics conducted. In Figure 1.1, a prototype of ultrasound imaging is presented.

Manual analysis for the diagnosis of diseases in echo-cardiographic images is difficult and consumes lot of time. Also, it is limited in terms of providing qualitative measure whereas automated analysis provides the exact numerical values to the factors that are required to judge the cases. In Figure1.2, a flow chart that describes the information that can be extracted using echo-cardiographic images is presented. There are variety of emerging techniques in the diagnosis of the cardiovascular diseases ranging from single-photon emission computed tomography (SPECT), positron emission tomography (PET) etc. Echo-cardiography has higher specificity when compared to other modalities. Moreover, the other advantages of echo-cardiography are it is inexpensive and it avoids the disadvantage of radiation exposure.

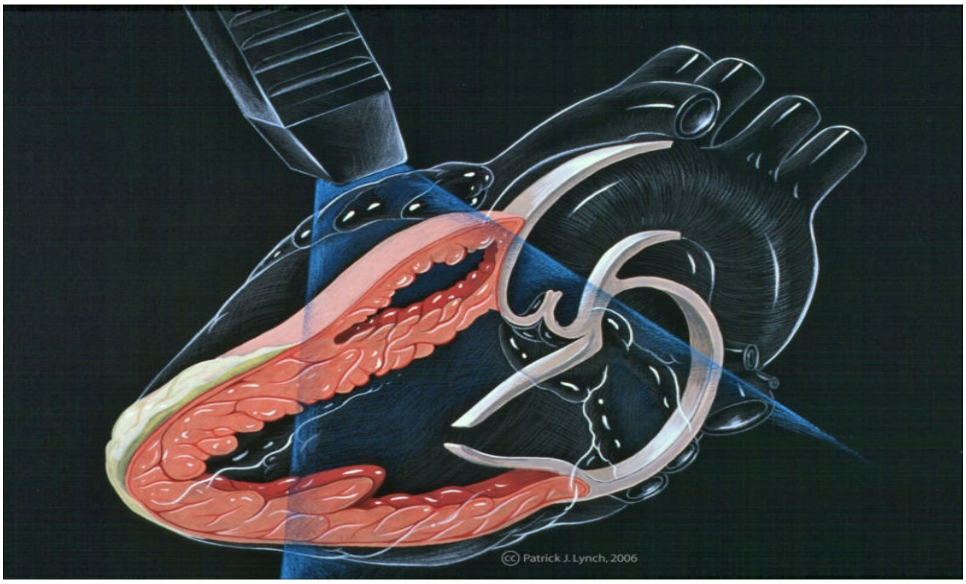

Figure 1.1: Prototype of Ultrasound Imaging

Echo-cardiography is most widely used techniques and there have been lot of technical improvements made in it since last two decades. It still remains a safe, inexpensive and accurate tool for the clinical diagnosis [2].

Diagnosis using echo-cardiographic images requires analysis of both movement and structure of the tissues present in them. In echo-cardiographic images, the displacement of the tissue from one frame to another frame is computed using different methods like segmentation [3–5], optical flow based [6, 7], registration based methods [8–11], speckle tracking [12–15] and other methods [16, 17]. In segmentation based methods a particular shape is segmented and then tracking of that particular shape is done in the images of the whole cycle. Optical flow, Image Registration and Speckle tracking methods compute displacement field at each pixel of the image. To detect the abnormalities in the echo-cardiographic images, information about movement as well as structure is important since it is required to assess the information about the the enlargement of the shape of heart or presence of any abnormality. Hence segmentation also plays a role in the diagnosis. Some of the diseases that can be diagnosed using the motion and structure are long standing hypertension, heart failure, cardiomyopathy, aknesia or dyskinesia, infections like rheumatic fever and other abnormalities like blood clots or tumours within heart [1, 18].

1.2 Problem Statement

The aim of this thesis is to develop techniques that aid automated diagnosis in echo-cardiographic images i.e., to provide information that helps doctors to evaluate the diseases based upon quantitative measures. This can be done by estimating the varying size of blood regions and tissue regions during the complete cycle of contraction and relaxation of heart. To achieve this, we need to be able to locate the tissue/blood regions(object) and the movement of them from one frame to another frame.

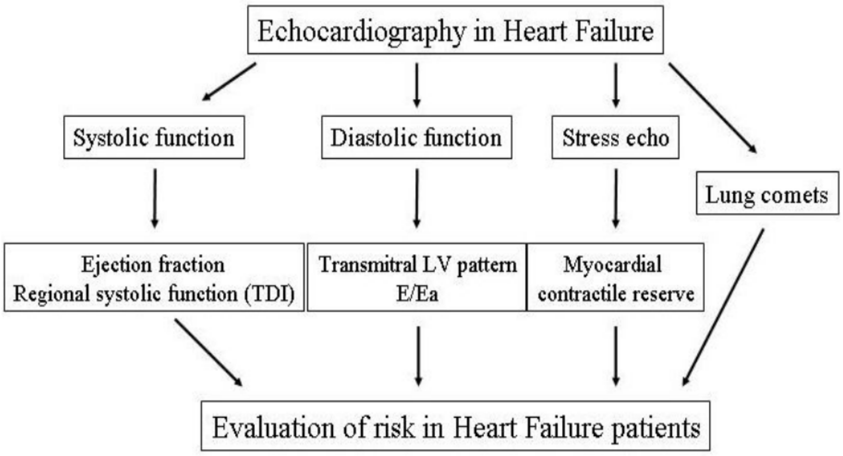

Figure 1.2: Role of Echo-Cardiography in Diagnosis

To analyse the echo-cardiographic images, some of the techniques present in computer vision and image processing are borrowed. Some of them are segmentation, registration and optical-flow based techniques. In segmentation, the pixels are grouped into regions based upon certain properties. Using the segmentation process the required region is segmented in all the frames and the change of the size of the required region is noted. But this approach only provides the information about shape and size of the heart. We also require the measure about the distance with which each pixel of the object is moving. One way to solve this problem is to go for image registration. Image Registration [19] is a process of establishing mapping between one or more images of the same scene acquired at different times, view points or modalities. The mathematical formulation of image registration is:

$$I_1(x) = I_2(T(x)) \tag{1.1}$$

where x is the pixel coordinates of the image, $I_1(x)$ is the Source Image, $I_2(x)$ is the Moving Image that is to be aligned with the source image and T is the mapping function.

Image Registration can be classified based upon the mapping function. If the mapping function between two images is linear then it is called rigid registration. It occurs when the variations present between the images is limited to illumination changes, perspective distortions and rigid movements in the objects i.e., one image can be mapped to other image using global affine transformation. If the variations between the images are more complex, like deformation of objects present in the image, then the mapping function will be non-linear, since linear function cannot handle it and this type of registration is called as non-rigid registration.

The mapping function in the case of echo-cardiographic images is non-linear because during its complete cycle heart undergoes a complex motion like twist, contraction and relaxation in the walls. To estimate this non-linear motion, we use free-form deformations, i.e, each pixel is given it's own

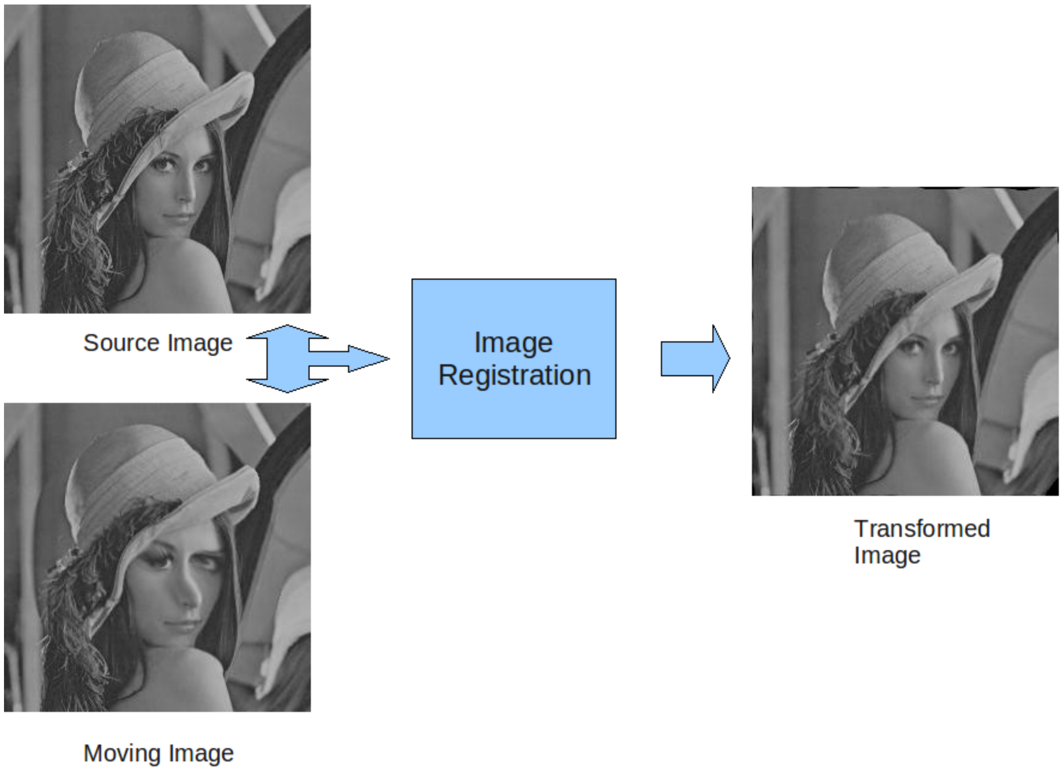

Figure 1.3: Example of Non-rigid Image Registration

displacement field (change in the position of pixel from one frame to another frame). An example of non-rigid registration is given in Figure 1.3.

In a similar way, we need to obtain the displacement field for the echo-cardiographic images. Analysis of echo-cardiographic images is difficult, because the images are of low contrast and have high speckle noise. The algorithms designed for the processing of these images either model the noise explicitly into the algorithm or use some pre-processing to filter out the noise. But due to pre-processing some information present in images is lost like the texture. The other kind of algorithms used induce the assumption that the echo-cardiographic images have multiplicative Rayleigh noise.

At the other hand, registration based algorithms implemented on echo-cardiographic images are quite a few, because of the presence of noise. The fundamental question addressed in this thesis is: Can standard registration algorithm be applied to echo-cardiographic images without pre-processing the image and without including the noise model into the algorithm?

The algorithm which we chose here is Demon's algorithm [20] for non-rigid registration. It is one of the standard registration algorithm for intra-modality images but hasn't been used for echo-cardiographic images. There have been lot of changes made to this algorithm but none of them addressed the problem of noise. We take this algorithm and modify it in such a way that it is robust to noise and it can be generalised to the other modalities also.

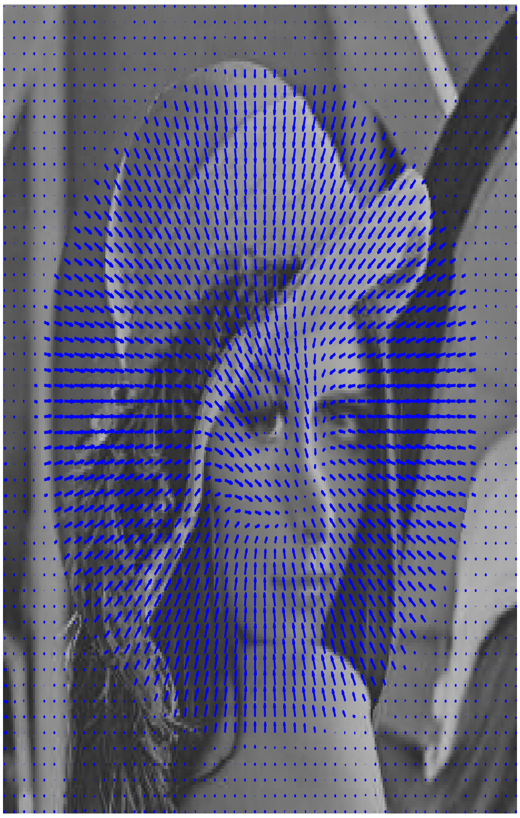

Figure 1.4: Displacement field computed for Source Image and Moving Image given in example of Non-rigid Image Registration in the above figure

1.3 Challenges and Motivation

The challenges that occur during the processing of echo-cardiographic images are due to the physics of acquisition of the images. Ultrasound waves are projected into the tissues and the reflected waves are acquired as an image. During their propagation through the tissue, these waves undergo three types phenomena: absorption, specular reflection and diffuse reflection. Echo-cardiographic images are noisy because of the diffuse reflection, it occurs when the size of scatterer present in the tissue is lesser than the wavelength of the acoustic pulse, then the scatterer reflects back the acoustic waves. Since there are many other scatterers present in the same tissue, there is an interference between the acoustic waves which are reflected back. The speckle noise in the echo-cardiographic images occurs because of this interference between the reflected acoustic waves.

1.4 Applications

The algorithms developed in this thesis can be used to further improve the accuracy in automated echo-cardiographic analysis. In addition to echo-cardiographic images, these algorithms can be used on images with high-level of speckle noise like SAR Images. Moreover, the basic technique used here also can be applied in the following applications:

- Shape detection in the images with high level of noise.
- Segmentation of required structures from the images.
- An additional feature for efficient image registration.

The core of the algorithms presented in this thesis can be used in many applications of image processing and computer vision. They are presented after the detailed explanation of the algorithms.

1.5 Organization of thesis

In Chapter 1, a broad overview of the thesis is presented. The major contributions of the thesis are introduced. The challenges involved in tackling the problem and the possible applications are discussed. Chapter 2 presents an overview of methods that can be used to solve the problem of thesis and a brief literature survey on those methods. Chapter 3 gives the background for reading the thesis. This gives detailed explanation of the most popular registration algorithm along with its different variations which makes it easier to understand the thesis.

In Chapter 4, the initial methods which were designed to solve the problem are presented. This provides enough background to understand how our solution is driven. In Chapter 5, the design of the algorithm for image segmentation is presented. Here, the advantages of using local-information at each pixel of the image is presented. This method performs well when compared to the algorithms which first de-noise/smooth and then process the images.

In Chapter 6, we tackle the problem of Image Registration with a new feature included in it. This algorithm is adapted from the traditional Demon's Algorithm and the addition of the new feature makes the algorithm more efficient in presence of speckle noise. These algorithms are tested in both synthetically generated noisy images and Original Echo-cardiographic Images. Finally the conclusion and the future work is presented in Chapter 7.

The contributions made in this thesis can be summarized as:

- Feature-space representation of Image using Radon-transform.
- Segmentation based upon a new technique on feature-space of an image and
- Inclusion of new features in image registration algorithm.

Chapter 2

Literature Survey

2.1 Introduction

The problem dealt in this thesis pertains to image analysis for identifying regions of interest in echo-cardiographic images. A brief literature survey is presented on the existing methods used for processing of echo-cardiographic images in this chapter.

There are several methods proposed over time which aim for image analysis in echo-cardiographic images. These methods can be broadly classified into:

1. Direct Methods which compute motion field for the whole image.
2. Indirect Methods which segment the image and then compute motion field.
3. Other methods which are based upon machine learning/image formation information.

The Direct Methods are those which compute the Dense-Motion field from one frame to other frame based upon intensity, statistics or other information from the image. The methods that fall into this category are Image Registration methods, Optical-flow based methods and Speckle Tracking methods. Indirect methods extract some features/prominent objects in the image and then compute the change in their size/shape from frame to frame. The methods that fall into this category are segmentation based. These methods compute sparse motion field. In this chapter, we present the literature survey on both Direct and In-direct methods for echo-cardiographic image analysis.

2.2 Direct Methods

These methods compute the displacement field between two consecutive frames. They are mostly based upon the optimization of an objective function which gives the information about how similar the two images are. Below is the brief description of the algorithms present in the literature.

2.2.1 Optical Flow

Optical flow is a representation of visual motion between two digital images. It associates each pixel with a velocity (v_x, v_y) which indicates the velocity between one image to other image. The velocity field is based upon local derivatives in a given sequence of images. In 2D, it specifies how much each image pixel moves between adjacent images while in 3D, it specifies how much each volume voxel moves between adjacent volumes. Optical flow algorithm assumes that intensity of a pixel is constant over the sequence of images (Brightness Constraint). Differential equation solving techniques are then used to compute the motion field, by solving additional constraints.

The brightness constraint assumption for an temporal image $I : (R^2, R) \rightarrow R$ in the computation of optical flow can be given as:

$$I(x, y, t) = I(x + \delta x, y + \delta y, t + \delta t) \tag{2.1}$$

i.e., for small displacements $(\delta x, \delta y, \delta t)$ the intensity is assumed to be constant.

Based upon Taylor's series expansion:

$$I(x + \delta x, y + \delta y, t + \delta t) = I(x, y, t) + \delta x.\frac{\partial I}{\partial x} + \delta y.\frac{\partial I}{\partial y} + \delta t.\frac{\partial I}{\partial t} + H.O.T \tag{2.2}$$

where $H.O.T$ is Higher Order Terms.

and then reducing the equation, we finally get

$$\delta x.\frac{\partial I}{\partial x} + \delta y.\frac{\partial I}{\partial y} = -\delta t.\frac{\partial I}{\partial t}$$

$$I_x.\frac{dx}{dt} + I_y.\frac{dy}{dt} = -I_t$$

However, we require additional constraints to solve this equation for motion field since there are two unknowns $(\frac{dx}{dt}, \frac{dy}{dt})$. The optical flow methods are classified as local and global based upon the additional constraints used. Horn Schunk [21] used a constraint based on global smoothness of the velocity field and minimized the following energy functional

$$\iint (I_x.u + I_y.v + I_t)^2 + \lambda(| \bigtriangledown u|_2^2 + | \bigtriangledown v|_2^2)\, dx\, dy \tag{2.3}$$

where $\bigtriangledown u = \frac{\delta u}{\delta x} + frac\delta u\delta y$ and $\bigtriangledown v = \frac{\delta v}{\delta x} + frac\delta v\delta y$ Lucas Kanade [22] used a local constraint. Here, the unknown motion field is assumed to be constant in a certain neighborhood. A least-square fitting is done in a small spatial neighborhood Ω by minimizing

$$\Sigma_{x,y\in\Omega} K_\rho * [\bigtriangledown I(x, y, t)]^2 \tag{2.4}$$

The optical flow techniques are used in a wide variety of applications because of its simplicity. These techniques are one of the earliest methods applied in echo-cardiographic images. Earlier techniques [6] assume a locally affine motion and extract the parameters from the motion field in small smooth regions of interest. In [23], three methods of optical flow which differ in the regularization(second constraint) terms are compared. Horn Schunk [21] and Lucas Kanade [22] performed better when compared with other techniques which are based on brightness-constraint.

A gradient-based hierarchical method is proposed in [7]. In this method, the images are pre-processed using a Adaptive weighted median filter[AWMF] proposed in [24]. The hierarchical method was introduced to cope with the noise present in the images.

In [25,26] optical flow which use gradient-based Horn-Schunck's method with additional constraints based upon motion estimates for characteristic surface points is proposed. In [27], the heart motion is modeled as local-affine model and the parameters are estimated by maximizing least squares inside a sliding spatio-temporal window by using B-spline smoothing function.

In [28], optical flow is introduced into the active contour based framework. Generally in active contour based method, the contour obtained in one frame is used as initial contour in the next frame, this doesn't hold true in the case of large displacement of the objects. Hence, a new initial contour is computed by applying optical flow displacement field on the previous contour.

In [29], Lucas kanade based optical flow is implemented for Real-time 3D Echo-cardiographic(RT3DE) data. The Left Ventricle Long Axis(LA) measurements obtained with the automated technique has been compared with LA measurements derived from manual selection of the LA from a volumetric display of RT3DE data. It showed a high-correlation of 0.99 between automated and manual selection of LA and performed better when compared to 2D echo-cardiographic data.

Statistical model is embedded into optical flow in [30] to take advantage of the time series. In [31] optical flow is computed upon the binary image obtained after boundary detection upon 2D echo-cardiographic data. The results presented are better than normal optical flow computed upon pre-processed data. In [32] the motion field obtained using optical flow is used to detect the abnormal motion in segments of the heart. In [33], the optical flow method is enhanced using Quasi-Gaussian DCT filter. Optical flow is also used in automated tracking in which it is combined with border tracking of cardiac motion models in [34]. Diamond search method with Brox's coarse-to-fine optical flow is proposed for Region of Interest tracking in echo-cardiographic images in [35]. A learning technique on optical flow propagation based upon Random Forest Trees is proposed in [36].

2.2.2 Image Registration

Image Registration is a process of establishing mapping between one or more images of the same scene acquired at different times, viewpoints or modalities. Image Registration methods can be classified into two categories based upon the approaches used: (1) Intensity based and (2)Feature based registration. These methods are further been classified into Rigid/Non-rigid depending upon the mapping function used in aligning the images. In Intensity based methods, an objective function is computed based upon the parameters of the mapping function to transform the images for alignment. The mapping function can be categorized as: rigid and non-rigid based upon the transformation present between the images. In Feature-based methods, the features are extracted from the images and they are mapped to compute the parameters for aligning two images. Intensity-based registration methods can be correlated to optical flow methods. Image Registration methods are very helpful for echo-cardiographic images since they provide flow-field between two images. Some of the Image Registration methods used for echo-cardiographic images are presented below.

The mathematical formulation of image registration is:

$$I_1(x) = I_2(T(x)) \tag{2.5}$$

where $I_1(x)$ is the source image, $I_2(x)$ is the Moving image that is to be aligned with the source image and T is the mapping function.

During its complete cycle, the heart undergoes a complex motion like twist, contraction and relaxation in the walls. Thus, the motion-field in echo-cardiographic images is also complex. Hence, the mapping function T used in the case of echo-cardiographic images is non-linear.

[37] proposed a segmentation with correlation in tracking. In [8], a deformable-model based registration was framed to estimate the dense motion field between the frames. In [9], a block matching based method is proposed where a local affine model is assumed and the parameters are estimated using least square basis. Non-rigid registration using b-splines has also been proposed in [10]. In [11], a novel non-rigid registration based method was proposed which includes intensity and phase information into the energy term which is to be minimized. Recently [38] proposed the non-rigid registration method with multi-resolution based optimization.

A new approach to estimate velocity field with spatio-temporally smooth velocity in diffeomorphic motion analysis is proposed in [39]. A variation of Demon's algorithm known as iLogDemons algorithm is proposed in [40].

2.2.3 Speckle Tracking

Speckle tracking method was first introduced in [12]. Here, optical flow is used to estimate the motion of speckle and the parameters of motion of the heart like rotation, deformation and translation which have been approximated by using a linear model for the velocities in a small window. The assessment was on real data in a small region of interest. Further an adaptive filter to remove speckle was introduced. Most of the methods use this in pre-processing step during the analysis of the echo-cardiographic images.

Speckle Tracking methods are developed specifically for echo-cardiographic images. These techniques are based upon tracking the speckle-noise present in the echo-cardiographic images. These methods use speckle-decorrelation to approximate the motion field between two images. The speckle noise in the images is modeled as a Rayleigh function/Complex functions and then used in the computation of the motion-field between the echo-cardiographic images.

In [13], a block-based optical flow was proposed. The displacement field was obtained using the maximum likelihood estimation assuming the multiplicative Rayleigh noise in the images. The method was compared by using Normalized cross correlation in the same framework.

Speckle tracking was also implemented on three-dimensional ultrasound data in [14]. This method is an extension of 2D speckle tracking but since the complexity is high, a dynamic programming based optimization was proposed. The method is evaluated upon a phantom such that it provides a benchmark for testing. In [15], a comparison of the accuracy of the speckle tracking based measurements of the heart with tagged Magnetic Resonance Images is presented and it is reported that the speckle tracking based methods provide a accurate measurements of Left Ventricle dimensions. In [41], the motion estimated by 2D speckle tracking method is compared with Cardio-MR and 3D Echo-cardiography. In [42] registration was based upon maximum likelihood estimation by assuming that the speckle statistics correspond to the Rayleigh distribution. The method was evaluated on ultrasound phantom and animal model using Sum of Squared differences.

Some of the new methods in speckle tracking include characterisation of speckle using Pearson Family of Distributions [43] and unsupervised clustering techniques for speckle detection in [44]. A combined method of shape and speckle tracking is presented [45]. There is also speckle tracking echo-cardiography introduced for automated diagnosis [46]. A speckle noise reduction method is proposed in [47].

2.3 Indirect Methods

In this category of Indirect methods, we only consider segmentation based approaches. Segmentation based techniques in echo-cardiographic images are aimed to extract a shape in one frame. This is then used in the approximation of the change in the shape of the object from frame to frame. Due to high-level of noise, segmentation based methods are mostly preferred in wall motion approximation.

2.3.1 Segmentation Based Methods

Early methods using segmentation include the pre-processing techniques combined with morphology. These techniques are still used recently in [4, 48]. Then Active contour based, active shape model based methods were introduced later and the improvements have been made on them. Active contour methods include [3, 49]. In Mikic et al. [3], active contours are used to segment a single frame and then the optical flow is applied on the obtained contours to initialize contours in the next frame. Jacob et al. [5] introduced a dynamic snakes based method to segment contours of Left Ventricle. In [50] active contour based segmentation along with curve fitting is proposed to speed up the segmentation process. Local entropy and anisotropic filtering is used to enhance pixel features for clustering in [51]. In [52], a statistical atlas of motion is built and used for automatic comparisons of motion patterns in echo-cardiographic images. Another interesting method is Region of interest segmentation [53] which is based upon weighted radial edge filtering. A semi-supervised approach for ultrasound images based upon Pearson distance between speckle features is proposed in [54].

The echo-cardiographic images have different types of speckle noise in different regions due to the differences in the reflection properties. These differences in the speckle noise can be used for the segmentation. One such method which segments the regions based upon differences in the probability distribution models of noise is proposed in [55]. Graph cut based segmentation was introduced in [16]. In this paper regions are extracted using graph cut algorithms and disease discrimination is done based upon matching of regional trajectories.

Active appearance model based segmentation is proposed in [56, 57] . In [56], pair wise active appearance model depicts the transition in motion phase through a Markov chain and the transition in both shape and appearance through a conditional Gaussian distribution. The joint Gaussian distribution of the shapes and appearances belonging to two consecutive motion phases (i.e., a pair of motion phases) is learnt from the database, from which the conditional Gaussian distribution is analytically computed. In [57], a novel extension of active appearance models (AAMs) for automated border detection in echocardiographic image sequences is reported. The active appearance motion model (AAMM) technique allows fully automated robust and time-continuous delineation of left ventricular (LV) endocardial contours over the full heart cycle with good results. In [58], a level set framework with shape and motion prior was proposed. This approach uses the following steps: rigid registration of the prior shape, level set segmentation constrained through the registered shape and region tracking. A constrained model based level set approach is proposed in [59]. Active contour model which uses Texture energy is proposed in [60]. Active contour model with convex function in which Rayleigh mixture model is used for differentiating inside and outside regions of an endo-cardium is proposed in [61].

In [62], Robust information fusion was used for combining matching results from multiple appearance models. Fusion is performed in the shape space to combine information from measurement and prior knowledge which is used for real time multi-mode tracking. In [63], images are segmented interactively and then initial correspondence is established using a shape-tracking approach. A dense motion field is then estimated using an anisotropic linear elastic model, which accounts for the fibre directions in the left ventricle. The dense motion field is in turn used to calculate the deformation of the heart wall in terms of strain in cardiac specific directions. Segmentation using deformable templates and Markov random fields is proposed in [17].

2.4 Summary and Conclusion

To summarize the methods present for echo-cardiographic image analysis are presented. There are two types of methods present: Direct methods which compute dense velocity field between two consecutive frames and Indirect methods which extract the prominent information from the frames and then analyze it over the frames. We have presented the list of all the existing methods in echo-cardiographic image analysis. Based upon their formulation, we can say that these methods require an additional step of pre-processing. The main aim in this thesis is to propose methods for analysis which do not explicitly model the noise or employ de-noising. The detailed description of the step-by-step formulation of the algorithm is given in further chapters.

Chapter 3

Background On Demons Algorithm

3.1 Introduction

The problem addressed in this thesis is to come up with algorithms for analysis of echo-cardiographic images. As a part of it, we explore the problem of Image Registration in this chapter. Image Registration is a process of alignment of two or more images of the same scene acquired at different times/viewpoints/modalities. Given two Images, the Image that is to be aligned with another Image is referred as Moving Image M and the Image which is used as target for aligning the Moving Image M is called as Source Image S. The deformation between these two images is mapped using Transformation function. Overall, the Image Registration process can be depicted in mathematical terms as:

$$S(x) = M(T(x)) \tag{3.1}$$

In the Image registration process, the pixel coordinates x of the Moving Image M are transformed using Transformation function T to align with Source Image S.

In this chapter, we present background on Demon's algorithm, that is used further in this thesis to design the algorithms. We chose Demon's algorithm because it is one of the most popular algorithms present for Non-Rigid Image Registration. Since the movement of heart is complex, echo-cardiographic images require Non-rigid Image Registration.

There are a wide number of techniques proposed for non-rigid registration which are inspired from various fields like information theory [64, 65], fluid theory [66, 67], optical flow [21, 68], splines [69] and block-matching [70, 71] etc. These techniques can be widely classified into:

1. *Feature-based techniques*: Here a set of prominent features present in the images like edges/ridges/salient points are extracted and matched based upon their geometric distance. Once the correspondences are obtained, the mapping function between the images is computed by interpolation of the displacement field;

2. *Intensity based techniques*: Here the parameters of the mapping function are obtained by the optimization of the similarity measure between two images. These similarity measures can vary

from Sum of Squared Difference, Cross-Correlation, Mutual Information etc.

3. *Iconic feature-based registration*: This falls in between feature-based and intensity-based techniques. Here, a similarity measure is used to pair the features in the images without pre-segmentation and geometric distance is used to find the transformation.

Demons algorithm proposed by Thirion [20] is one of the popular non-rigid image registration method which is designed as a set of components which can be changed according to the requirement. The algorithm is inspired from the diffusion process present in theory of thermo-dynamics. Image registration can be assumed as a diffusion process. In this process, the source image is the stable state obtained at the end of diffusion process and the moving image is the initial state of the process which has the mixture of particles. Hence, the problem of aligning two images now becomes a diffusion process in which moving image is diffused into source image.

3.2 Method

First, we explain the diffusion process and then explain how it is used in Image Registration. The concept of demons in the diffusion process was introduced by Maxwell to illustrate a paradox of thermodynamics. Suppose, we have a mixture of two types of gas particles, type a and type b, seperated by a semi-permeable membrane. We also assume that the semi-permiable membrane which contains a set of particles called as demons, which are capable of distinguishing between the two types of particles, and allow particles of type a only to diffuse to side A of the membrane and particles of type b only to diffuse to the other side B. Hence at the end of process of Diffusion, side A contains only particles a, and side B contains only particles b.

Below we present the details of the diffusion used in Demon's algorithm. The problem of registration is to align the Moving Image M with the Source Image S i.e., M is to be deformed to match S. We assume that the contour of an object O in S is a membrane, and all the demons are scattered along this contour. Moving Image M is assumed to be a deformable grid, whose vertices are particles which can be classified as 'inside'or 'outside'particles with respect to the contour O in the Source Image S by the Demon particles. The Demon's push each of the vertices in the M 'inside'or 'outside'and then by the end of the registration process, we have M aligned with S.

The four components of Demons Algorithm can be given as:

1. Selection of Demons: The demon points $P \in D_S$ (set of Demon Points) can be present anywhere on the Source Image S, all pixels, contour points etc.

2. Transformation Model: The Transformation model T can be rigid, affine, spline or free form etc.

3. Interpolation: The interpolation method is needed to estimate T for the non integer positions $T^{-1}(P)$ it can be linear, spline etc.

4. Computation of the Demon Force: The force equation at each demon which can be of constant magnitude, based upon gradient or optical flow.

The demons P placed at the semi-permeable are the key effectors of the registration process. The moving image is assumed as a deformable grid M and the Demons are pushed based upon the difference of the intensity i.e., the new positions of the Demon's are computed based upon the force equation. The whole registration process is carried out in an iterative process where a small δT_i is added to T_{i-1} at the end of each iteration. δT_i depends upon the forces exerted by the demons on the pixels(particles) of the moving Image. The moving image is registered when the forces at the demons is equal to zero.

The framework of the Demons algorithm is given in Figure 3.1

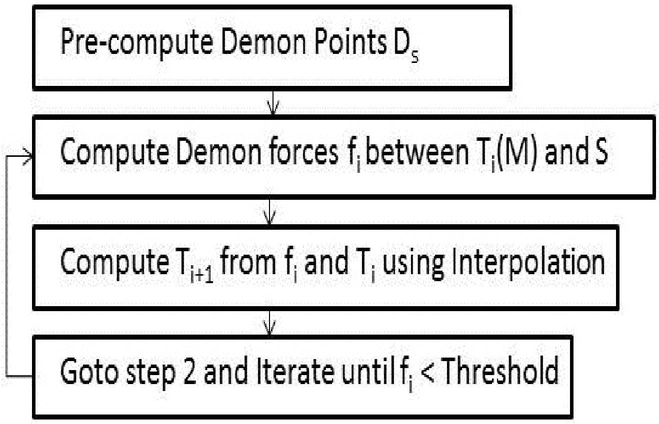

Figure 3.1: Pipeline of Demons Algorithm

The initialization of the process is done with T_0 at the first iteration. At the i^{th} iteration, we have estimated T_i and we need to compute T_{i+1}, which is composed of two steps:

1. For each demon $P \in D_s$, compute the associated elementary demon force $f_i(P)$ which depends on the demon direction ds at point P and on the polarity of M at point $T_i^{-1}(P)$.

2. Compute T_{i+1} using $T_{i+1} = \delta T_i + T_i$. The addition δT_i is computed from all the elementary demons forces $f_i(P), P \in D_s$.

Based upon the location of the demon particles, the algorithm has three variations:

- All pixels in the image,
- Pixels present on the features like edges, ridges etc. and
- Pixels separating two labeled regions obtained after segmentation.

The detailed explanation of these variations of Demon's algorithm are presented in the sections below.

3.2.1 All pixels are selected as Demons

1. The set of Demons D_s is the set of all pixels of the source image i.e.,$D_s = S$.

2. Transformation model is a free-form deformation i.e, each demon point P is assigned with a displacement field $d(P)$. To get a smooth field, a Gaussian filter is applied to the whole field.

3. The value at position P' in M, where $P' = P + d(P)$ is estimated using tri-linear interpolation.

4. The demon force is given by the optical flow, the displacement $\mathbf{d} = -\mathbf{v}$ where $\mathbf{v}$ is the velocity obtained. A detailed description of optical flow is given below:

Optical flow Method computes the flow-field between two temporal images taken at different time frames. There are a variety of optical flow methods proposed which can be classified as differential based, region-based, energy based and phase-based techniques. The displacement field computed in Demon's Algorithm is borrowed from differential based techniques. Differential based techniques compute the flow-field using the spatio-temporal derivatives of the image intensities.

The basic assumption made in Optical-flow is that the intensity remains constant during a small displacement. Let $I : (R2, R) \rightarrow R$represent the set of temporal images. The brightness constraint assumption made in the computation of flow-field in Optical-flow algorithm is:

$$I(x, y, t) = I(x + \delta x, y + \delta y, t + \delta t) \tag{3.2}$$

at pixel (x, y) and time frame t

i.e., for small displacements the intensity is assumed to be constant.

From Taylors Expansion we have,

$$I(x + \delta x, y + \delta y, t + \delta t) = I(x, y, t) + \delta x.\frac{\partial I}{\partial x} + \delta y.\frac{\partial I}{\partial y} + \delta t.\frac{\partial I}{\partial t} + H.O.T \tag{3.3}$$

where $H.O.T$ is Higher Order Terms.

By equating the above two equations we have:

$$\delta x.\frac{\partial I}{\partial x} + \delta y.\frac{\partial I}{\partial y} = -\delta t.\frac{\partial I}{\partial t}$$

$$I_x.\frac{dx}{dt} + I_y.\frac{dy}{dt} = -I_t$$

$$\bigtriangledown I.(u, v) = -I_t \tag{3.4}$$

where $\bigtriangledown I = \begin{bmatrix} I_x \\ I_y \end{bmatrix}$

and $(u, v) = \begin{bmatrix} \frac{dx}{dt} \\ \frac{dy}{dt} \end{bmatrix}$

However, this equation is not enough to compute the flow-field since we have two unknowns (u, v) and one equation. There is a need of additional constraints to compute the flow-field. The additional constraints proposed can be classified as local methods and global methods.

The constraint is same as Horn Schunk based method [21] where is based on the global smoothness of the flow-field. The energy functional which is minimized in this method is:

$$\iint_k (\triangledown I.U + I_t)^2 + \lambda(| \triangledown U|_2^2 + | \triangledown v|_2^2)\, dx\, dy \tag{3.5}$$

where k is the index of the pixels in the neighborhood of (x, y).

The first term in the equation denotes the brightness constraint and the second term denotes the global smoothness constraint i.e., the gradient of the velocity is minimum (the changes in the velocity is constant). At the end of derivation, the equations for velocities at kth iteration are given as:

$$\mathbf{v} \approx -G^{-1}b \tag{3.6}$$

where

$$G = \Sigma_k \begin{bmatrix} I_x^2 & I_x I_y \\ I_x I_y & I_y^2 \end{bmatrix} \tag{3.7}$$

and

$$b = \Sigma_k \begin{bmatrix} I_x I_y \\ I_x I_t \end{bmatrix} \tag{3.8}$$

The details of the derivation can be given in [21].

3.2.2 Demons present on contours

1. Demons are placed at the edge locations of the Source Image S and hence displacement field is calculated at the edges.

2. Since the displacement field is only present at Demon, the displacement at other pixels is computed by using Global transforms (rigid, affine) [72] as Transformation function. Deformations are modeled using warping techniques [73] which extend the displacement obtained at D_s to all the remaining pixels in the source image.

3. The interpolation done is tri-linear similar to the one in the above method.

4. The demon force computation is described below:

The displacement field at each demon point P is oriented in the direction of normal of the contour which is given as $\mathbf{n} = \frac{\triangledown(\mathbf{P})}{|\triangledown(\mathbf{P}|}$. The force equation P is formulated in terms of $S(\mathbf{P})$ intensity at Position $\mathbf{P}$, S_{in} which corresponds to the intensity of the pixels inside the contour in the direction of normal and S_{out} which corresponds to the intensity of the pixels outside the contour in the opposite direction of the normal. If $S(\mathbf{P})$ is less than S_{in}, then the Demon point is pushed towards inside direction of the contour i.e., displacement vector is equal to the normal pointing inwards with maximum magnitude. If

$S(\mathbf{P})$ is greater than S_{in} and less than S_{out}, then the magnitude of the displacement vector is computed by taking the ratio of the present intensity difference and the intensity difference of inside and outside regions. When the intensity $S(\mathbf{P})$ is greater than S_{out}, then the Demon point P is pushed towards outside direction of the contour i.e., displacement vector is given the maximum negative magnitude along the normal vector pointing outwards.

Then the magnitude of the demon force in terms of mathematical equation is calculated as:

$$\mathbf{f}(P) = K_{s_{in},s_{out}}(m(P'))\mathbf{n} \tag{3.9}$$

where

Inside Intensity $S_{in} = S(P + k\mathbf{n})$

Outside Intensity $S_{out} = S(P - k\mathbf{n})$

K is a constant possibly 1.

The equation can be well depicted in Figure **??**

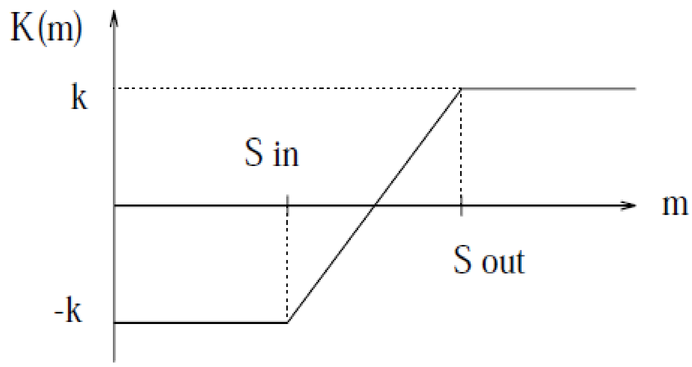

Figure 3.2: K function

From this equation, it is clear that the demon pushes inside if the intensity belongs to the inside $(K < 0)$ of the contour else it pushes outside $(K > 0)$. There are some more variations made in the K function which are almost similar to the above.

3.2.3 Demons at the pixels separating two labeled regions

1. The pixels whose adjacent labels are different are selected as demon points.

2. The transformation model is similar to the second method(Demons present on contours).

3. The label of the nearest pixel is used.

4. The demon force computation is described below:

When the source image is segmented, the demons are the points which separate two regions having different labels. Then the demon force is given by checking the labels of the Moving Image M with the labels of s_{in} and s_{out}. These are described below:

- If $m \neq s_{in}$ and $m \neq s_{out}$, $\mathbf{f} = 0$.
- If $m = s_{in}$, $\mathbf{f} = -k\mathbf{d}$
- If $m = s_{out}$, $\mathbf{f} = k\mathbf{d}$

If the label belongs to the object then it is pushed inside in the direction of the normal else it is pushed in the opposite direction.

3.3 Analysis of Each variation

Since the maximum probability of occurrence of error is in computation of the displacement field, we discuss the accuracy of each variation in the below sections:

3.3.1 Optical flow

The displacement field is computed at each and every pixel based upon the computation of the optical flow which is based upon the brightness constraint. This works very efficiently in ideal case but in presence of noise, it fails to perform well because of the brightness constraint. Since every pixel has a displacement vector the actual displacement might get affected because of the uncertainty caused by the displacement vector, at each pixel.

3.3.2 Demon Force at edges

Correctness of the displacement field depends upon the selection of the features. Computation of the displacement field assumes that the intensity varies linearly along the features, therefore the pixels having high intensity difference have high displacement and the pixels having low intensity have low displacement, which may not be true in all cases.

3.3.3 Demons separating two labeled regions

In this case, both the Source Image S and Moving Image M are segmented and labeled. The demons are present along the boundaries separating two labeled regions. The displacement field now is a constant, which is pointing towards the inside region or the outside region depending upon the label of the pixel in the moving image. This method relies on the segmentation method used on the image.

3.4 Summary

In this chapter, an overview of Demons algorithm is presented. Since demons algorithm is one of the most widely used methods for non-rigid image registration, we carefully analyze all the three variations of the Demons algorithm. The source of the displacement equations in the Demons Algorithm and the reasons for the failure in presence of noise for each case of Demons Algorithm is presented. In the next chapter, we discuss the possible variations that can improve the Demons Algorithm for image registration.

Chapter 4

Possible Improvements On Demon's Algorithm

4.1 Introduction

The aim of our work is to design an efficient motion estimation algorithm which can handle the noise present in the echo-cardiographic images. The approach we chose is non-rigid registration since it allows computation of dense-field estimation which can represent the complex motion of the heart. The success of any registration algorithm lies in the accuracy of the displacement field computation and regularization of the obtained displacement field. Demon's algorithm is one of the most efficient algorithm for intramodal image registration, but when applied to echo-cardiographic images it fails because of the presence of high level of speckle noise. In the sections below, we present some solutions for handling noise in the Demons Algorithm framework. We begin by describing the source of noise in echo-cardiographic images.

4.2 Source of Noise

Echo-cardiogram is acquired by transmitting high-frequency sound waves into the tissue to be imaged. When the sound waves travel through the tissue, some of the waves are reflected back by the tissue which are recorded as an echo-cardiographic image. Thus, an echo-cardiographic image represents the strength of the echoes.

Usually a transducer is used to emit the acoustic pulses into the tissue. The transducer has peizo-electric elements which convert electrical energy into acoustic energy and acoustic energy to electrical energy. Same tranducer is used to both transmit and receive the acoustic pulses.

When an acoustic pulse travels through the tissue it can undergo one of three processes : absorption, specular reflection and diffuse reflection. Absorption occurs due to the fact that particles of the wave require some energy to travel through the tissue and this energy which is lost depends upon the attenuation coefficient specific to each medium. Each tissue type also has a characteristic acoustic impedance to the acoustic wave. Hence, the type of the tissue is characterized by the change in the acoustic impedance.

This is the reason why the pulse is reflected back at the boundary of the tissues. This phenomenon is called as specular reflection.

The noise in the echo-cardiographic images is because of diffuse reflection. This type of reflection occurs when the size of scatterer present in the tissue is lower than the wavelength of the acoustic pulse. The acoustic waves which result from diffuse reflection by several scatterers undergo interference and give rise to speckle noise.

4.2.1 Noise Model

The echo-cardiographic image represents the strength of the back-scattered echoes. Hence if we model the echo reflected by each scatterer then the intensity at a particular pixel in the image is nothing but the sum of the echoes back-scattered by all the scatterers present in the resolution cell, which is the smallest unit of the tissue through which the incident sound wave travels. Denoting an acoustic pulse with uniform frequency P_0 can be written as

$$P_0 = a.\cos(w_0 t) \tag{4.1}$$

where a is the amplitude and w_0 is the frequency of the wave

When this wave is backscattered by a scatterer then the quantities that are effected are the amplitude and the phase. Amplitude depends upon the medium of the scatterer. Hence the reflected echo from the ith scattetter P_i is given as:

$$P_i = \alpha_i.\cos(w_0 t + \phi_i) \tag{4.2}$$

The signal received at a particular pixel in an echo-cardiographic image is the sum of the echoes reflected by each scatterer present in that resolution cell which can be given as:

$$s = \Sigma_{i=1}^{n}(\alpha_i \cos(w_0 t + \phi_i) \tag{4.3}$$

$$s = \Sigma_{i=1}^{n}(\alpha_i(\cos(w_0 t).\cos(\phi_i) - \sin(w_0 t).\sin(\phi_i))) \tag{4.4}$$

But the scatterers present in the resolution cell are very large and are randomly distributed in the resolution cell. Hence the unknowns in the above equation can be modelled as random variables

$$s = X\cos(w_0 t) - Y\sin(w_0 t) \tag{4.5}$$

where

$$X = \Sigma_{i=1}^{n}(\alpha_i.\cos(\phi_i))$$

$$Y = \Sigma_{i=1}^{n}(\alpha_i.\sin(\phi_i))$$

By central limit theorem, if there are large number of scatterers then the random variables X and Y can be approximated using Gaussian distribution model. The envelope signal now becomes sum of two Gaussian distributed models which is Rayleigh distribution. There are other distribution models proposed that represent both largely and scarcely distributed scatterers. The detailed description of noise models is presented in [74–78].

4.3 Drawbacks of Demon's Algorithm

The drawbacks of Demon's Algorithm are:

- Borrows the displacement field computation from optical flow.
- Sensitive to noise.
- Sensitive to error present in gradient computation.

The possible modifications for the improvement of this algorithm are presented below, where the improvement is in terms of increase in robustness to noise.

4.4 Possible Modifications

Modification 1 The source of the noise sensitivity is the brightness constraint underlying optical flow computation. So, an option is to replace this constraint using a probabilistic model as proposed in [79]. However this model calls for an explicit noise-modelling step. Since noise-model varies with modality, different models have to be considered according to the modality. The details of experimenting in this variation is reported later in this chapter.

Modification 2 Employing different features to represent the image regions. Since different regions in Ultrasound Images have different probability distributions because the number of scatterers present differ from tissue to tissue [78]. Hence different features like Edge-map and other feature descriptors can be used. The different ways of using features are presented below:

- One alternative is to compute an optical-flow on an edge-map. This has been reported in [31]
- Use of feature descriptors like SIFT / Geometric Blur which provide information of the image in multi-scales.
  This method is further explained in the next chapter.

Modification 3 Variation of the displacement field in the regularization step. Normally Gaussian smoothing is used in regularization of the displacement field. But these regularization methods can be tried only after the computation of the displacement field. This step can be thought of as filtering process after the displacement field is obtained:

- In the case of dense displacement field, we take a dominant displacement vector in a small neighborhood, to avoid noisy displacement field.
- In the case of contour based demons, computation of the displacement using multi-scale image pyramid.

Modification 4 Computation of displacement using region-based matching method. But the displacement field is computed only at the boundaries of the regions, then the displacement field at other pixels is calculated using Interpolation methods.

Next we present the details and the results of the first variation i.e., including probabilistic brightness constraint model into the demon force computation. The details of second variation are presented in next Chapter. Third and fourth variations are out of scope of this thesis.

4.5 Probabilistic Brightness Constraint Model

[79] presents three significant issues of optical flow methods, they are:

1. The brightness constraint is derived using a first-order Taylor approximation implying that the flow magnitude is assumed to be small. However many algorithms neglect this fact and use this underlying assumption as an algebraic line with infinite extent.

2. It assumes that the image derivatives observed are true valued. Therefore the existence of noise in the observed image is not considered explicitly.

3. The derivation of the brightness constraint is itself based in an incorrect manner where the temporal dimension is treated differently from the spatial dimensions. This may be because early methods of optical flow were used for the data where only two images were available and the time-step was assumed to be 1.

In [79] a correct approach for modeling the spatio-temporal volume in a uniform and continuous manner is proposed. It introduces the specific discretization of the spatio-temporal image data only as an algorithmic detail. This approach is recasted into well-known flow algorithms to convert them into more accurate versions.

The solution is developed by assuming a continuous space-time image volume, correct estimation for flow is not a two-dimensional vector but its homogeneous part in the normalized volume flow. Let the estimated derivatives of Images I be $I_d = [I_x, I_y, I_t]^T$.

The error in the image derivatives is presented using the additive Gaussian noise model

$$I_d = I_{d0} + n \tag{4.6}$$

where I_{d0} is the true Image derivatives and $n = [n_x, n_y, n_t]$ is the noise term

Using the brightness constraint we have,

$$I(x+U, y+V, t+W) = I(x, y, t) \tag{4.7}$$

$$I(x, y, t) + \frac{\partial I}{\partial x}.U + \frac{\partial I}{\partial y}.V + \frac{\partial I}{\partial t}.W = I(x, y, t) \tag{4.8}$$

$$\frac{\partial I}{\partial x}.U + \frac{\partial I}{\partial y}.V + \frac{\partial I}{\partial t}.W = 0 \tag{4.9}$$

$$I_d^T.F = 0 \tag{4.10}$$

where

$$F = \begin{bmatrix} U \\ V \\ W \end{bmatrix} \tag{4.11}$$

It can be seen that we have an unknown scale factor for F , i.e., $I_d^T.F = I_d^T(\alpha F) = 0$, implying that we can only derive F upto a scale factor. Hence the scale is fixed using normalized volume-flow vector $f = \frac{F}{|F|}$.However Equation (4.6) holds true only when the image derivatives have true values, whereas we have only estimated derivatives.

A conditional distribution of flow is given using the chain rule for conditional probabilities and using the relationship

$$I_{d0}^T.F = (I_d - n)^T.F = 0 \tag{4.12}$$

The conditional probability equation is given as

$$P(F|I_d) = \int \underbrace{\delta(I_{d0}^T F)}_{P(F|I_{d0})} \underbrace{e^{-\frac{1}{2\sigma^2}(n_x^2+n_y^2+n_t^2)}}_{P(I_{d0}|I_d)} dn_x dn_y dn_t \tag{4.13}$$

The brightness constraint is valid only for true image derivatives, it implies that only flow values that satisfy this equation are admissible. Therefore the conditional probability $P(F|I_{d0})$ is described by the brightness constraint and given as $\delta(I_{d0}^T F)$ where $\delta(.)$ is the Delta function. Since the error present in the true derivatives is represented using Gaussian noise the conditional probability $P(I_{d0}|Id)$ by using the Gaussian noise prior. Thus $P(I_{d0}|I_d) = \exp(-\frac{n^T n}{2\sigma^2})$ where $n = [n_x, n_y, n_t]$ represent the noise in the image derivatives.

By substituting these values from (4.6) and expanding the constraint into respective terms we get

$$I_{d0}^T F = I_d^T F - (n_x U + n_y V + n_t W) \tag{4.14}$$

to solve for the integral.

$$P(F|I_d) = \frac{1}{|W|} \int e^{-\frac{1}{2\sigma^2}(n_x^2+n_y^2+\frac{(n_x U+n_y V-c)^2}{W^2})} dn_x dn_y \tag{4.15}$$

The final equation obtained is:

$$P(F|I_d)\alpha \frac{e^{-\frac{1}{2\sigma^2}\frac{(I_x U+I_y V+I_t W)^2}{U^2+V^2+W^2}}}{\sqrt{U^2+V^2+W^2}} \tag{4.16}$$

The probabilistic model for brightness constraint is obtained, but now we need to compute the displacement field using this new model. In this paragraph explanation of incorporating this model into Lucas-Kanade framework is given. In Lucas-Kanade algorithm the error for each patch is:

$$E = \sum_k (I_x^k u + I_y^k v + I_t^k)^2 \tag{4.17}$$

where k is the index of the individual pixels in the patch.

The solution for the minimum value of E in Lucas Kanade is given as:

$$\max_f \prod_k P(f|I_d^k) \Rightarrow \min_f e^{-\frac{1}{2\sigma^2} f^T (\sum_k M_k) f} \tag{4.18}$$

The estimated flow is the eigen value of the following matrix

$$\overline{M} = \frac{1}{N}\sum_{k=1}^{N} M_k = \frac{1}{N}\begin{bmatrix} \overline{I_xI_x} & \overline{I_xI_y} & \overline{I_xI_t} \\ \overline{I_xI_y} & \overline{I_yI_y} & \overline{I_yI_t} \\ \overline{I_xI_t} & \overline{I_yI_t} & \overline{I_tI_t} \end{bmatrix} \tag{4.19}$$

For a constant flow over a patch, using the probability distribution equation

$$P(f/patch) = \phi_k P(f/I_d^k) \tag{4.20}$$

The flow is estimated by maximizing the conditional probability distribution

$$P(.) = e^{-\frac{1}{2\sigma_f^2}\frac{U^2+V^2}{U^2+V^2+W^2}} = e^{-\frac{1}{2\sigma_f^2}\frac{f^TDf}{f^Tf}} \tag{4.21}$$

The estimated flow is given as, which is the smallest eigen-vector matrix,

$$\overline{M}_{map} = \frac{1}{\sigma_n^2}NM^- + \frac{1}{\sigma_f^2}D \tag{4.22}$$

This displacement field is now used in the first variation of Demon's algorithm in Demon force computation.

4.6 Experiments

The modified Demons algorithm is implemented with the following parameters. The patch size is selected as 3 so that the displacement field computed doesn't get effected by the noise present in the neighborhood. The no. of iterations is 400, though the algorithm converges at 100 iterations, a high convergence criteria is used to get good results. The performance is evaluated for synthetic images for both with and without noise images. Both qualitative and quantitative results are presented below. For original echo-cardiographic images, we use pre-processing techniques since these echo-cardiographic images have high level of speckle noise in addition to the noise present during computation of the derivatives.

4.6.1 Data

The algorithm has been tested for synthetic images with and without noise. This is done to analyse the performance of the algorithms in presence of noise.

Synthetic Data 1

The first set of synthetic data has four images. Each single image has a dark circle in the white background. The intensity inside the circle varies inversely according to a Gaussian function i.e., at the center it is zero and as we move away from the center the intensity increases. The first image has a radius of about 25 pixels and it decreases uniformly in the next 3 images. No noise is added to these images.

Figure 4.1: Filtered Image using Wavelet De-noising Techniques

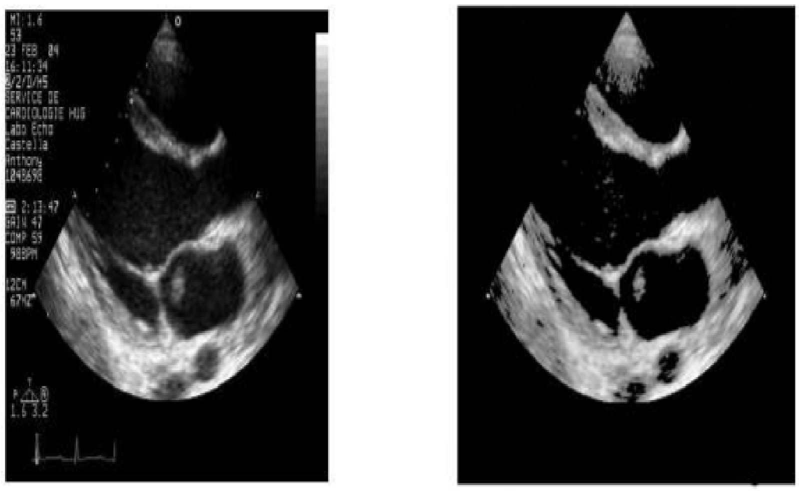

(a) Original Image (b) Filtered Image

Synthetic Data 2

In the second synthetic dataset, a random shape is created on a black background. The intensity of inside the random shape object is multiplied with a Gaussian function. This shape of the object is shrinked from one frame to another frame. Five such frames are created. To test the robustness of the algorithms we add Gaussian noise at with increasing variance to all the images. We present the SNR noise ratio of the images along with the results obtained.

Original Data

The efficiency of the proposed algorithm is also tested on the original echo-cardiographic data. Due to the presence of high level noise we use a pre-processing step to filter the noise. The algorithm used for pre-processing is based upon standard wavelet de-noising techniques. It uses non-orthogonal wavelets and ensures that the phase information is preserved in the image. In the Figure 4.1 we present the Original image and the filtered image.

4.6.2 Validation

The obtained results are compared with three different algorithms namely Optical flow, Probabilistic Model based Optical flow and Demon's algorithm.

Evaluation Measure

The evaluation measure used to compare the accuracy of the algorithm is sum of squared difference between the Registered Image and the Source Image.

$$SSD = \frac{(I_r - I_s)^2}{\text{Total no. of pixels in the Image}} \tag{4.23}$$

where I_r is the obtained image after registration and I_s is the source image.

Results

In our implementation we use the parameter settings mentioned below. The neighbourhood region in which the optical flow is computed is 3. We use two convergence criteria for the registration algorithm: 1.number of iterations is limited to 400 iterations and 2. displacement field computed by the algorithm is less than 0.5 for 20 continuous iterations.

First we present the results obtained on the first synthetic dataset. Figure 4.2, shows the three sets of source image And moving images. Figure 4.3, shows the results obtained on the synthetic data using four different algorithms. The images are arranged column-wise, the first column has the Registered images obtained by Lucas Kanade Optical Flow, second column corresponds to the registered images obtained using Probabilistic framework for optical flow, third column corresponds to the standard first variation of Demon's algorithm and the fourth column corresponds to the proposed algorithm. In Figure 4.4, the displacement field for one image pair is shown.

Qualitative results show that optical flow and demons algorithm give the registered images which are similar to source image. The artifacts present in the registered images obtained from optical flow and demons algorithm are very minor when compared to that of probabilistic optical flow. The proposed algorithm shows more artifacts because here the displacement field is computed in an iterative way when compared to normal optical flow. Therefore if there is an error in the computation of displacement field, it gets added up iteratively. However we can see the swirl pattern in the probabilistic framework of optical flow.

Now we present the results on the second synthetic dataset. In this data noise is added to the same source and moving images used in the first synthetic dataset, the noise level increases from left to right in each row. All the input images are presented in Figure 4.5. The first row corresponds to the source images and the second row corresponds to the moving images. In Figure 4.6, the transformed images using the four algorithms are placed columnwise. The first column is the output of Lucas Kanade Optical flow, second column is the output of Probabilistic Optical flow, third column is the output of Demons algorithm and the fourth column is the output of Demons algorithm. The displacement field is overlayed on the Moving image is present in Figure 4.7. First row has two images in which one of them is the displacement field of Optical flow and the other is the output of Probabilistic optical flow. Similarly the second row has the output of Demon's algorithm and the proposed algorithm.

The results show that Optical flow and Probabilistic Optical flow have better results when compared to Demons and Proposed algorithm. The reason can be the addition of displacement field in each iteration.

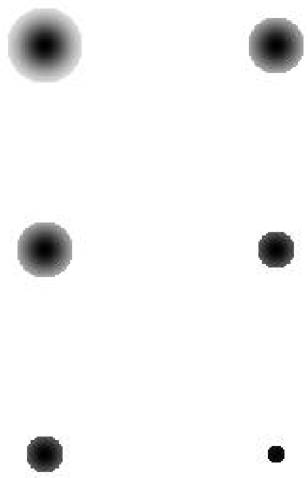

(a) Source Images (b) Moving Images

Figure 4.2: Corresponding pairs of input Moving and Source Images for Registration algorithm

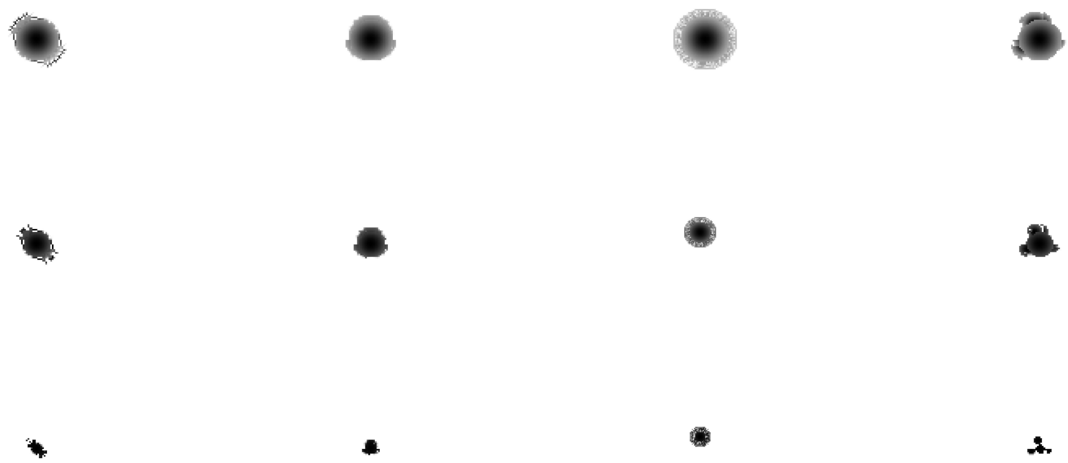

(a) (b) (c) (d)

Figure 4.3: Transformed Images obtained from Optical flow and Image Registration algorithms (a)Lucas Kanade, (b)Probabilistic Optical flow, (c)Demon's Image Registration Algorithm and (d)Proposed Algorithm

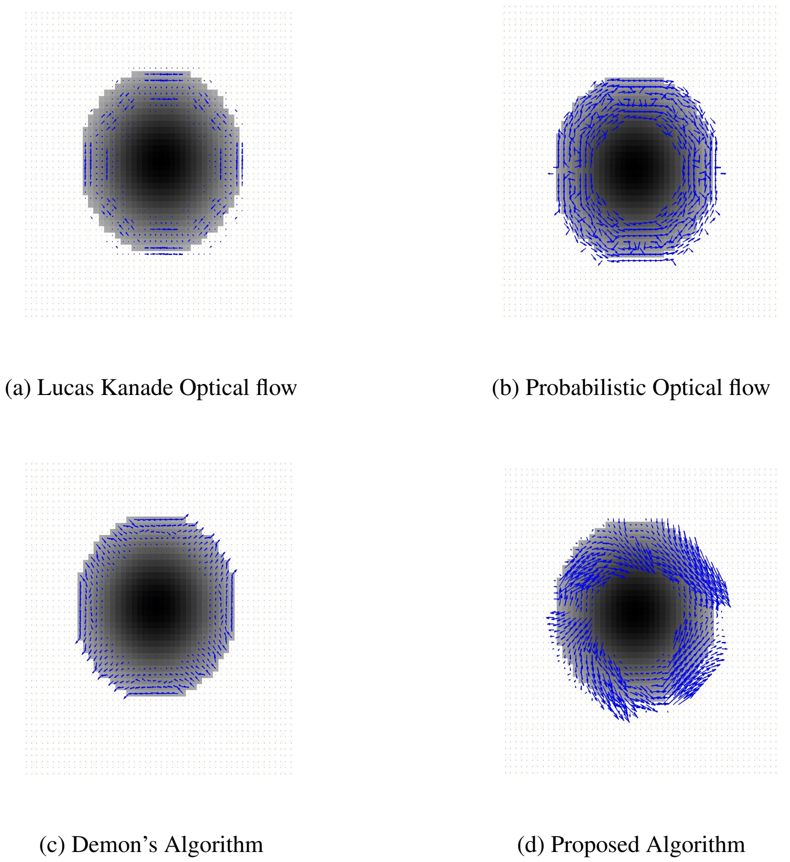

(a) Lucas Kanade Optical flow

(b) Probabilistic Optical flow

(c) Demon's Algorithm

(d) Proposed Algorithm

Figure 4.4: Displacement field obtained using Optical flow and Image Registration algorithms

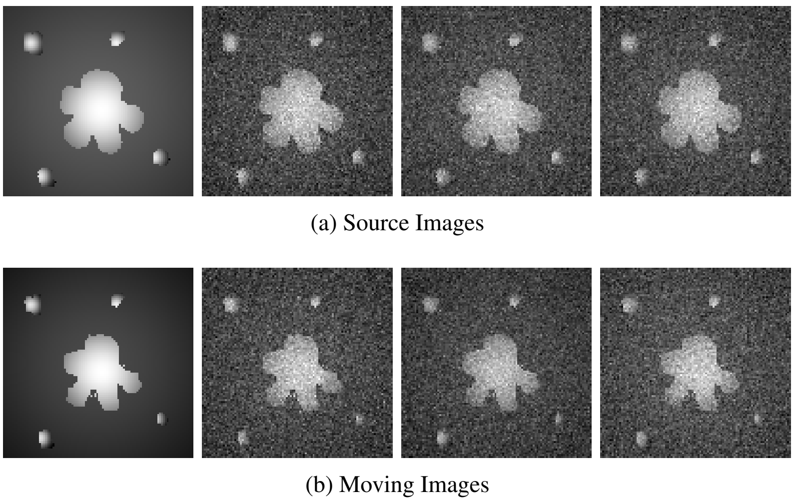

(a) Source Images

(b) Moving Images

Figure 4.5: Input Images for Optical flow and Image Registration Algorithms

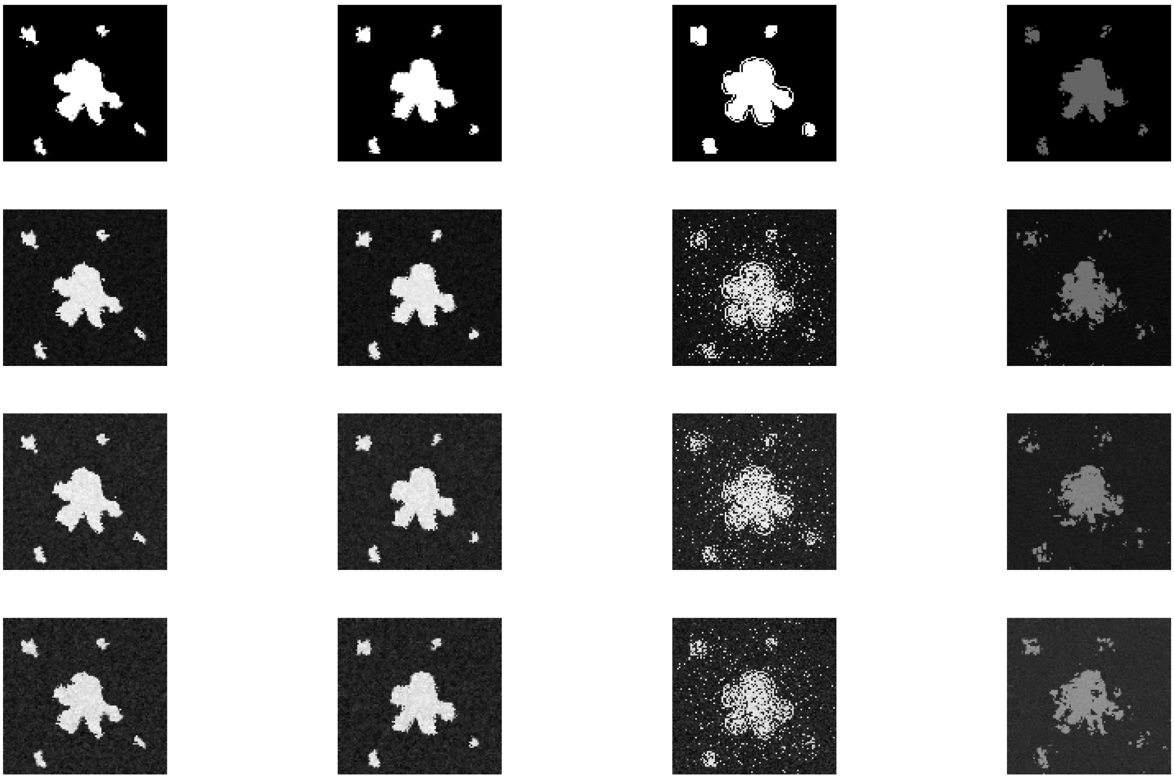

(a) (b) (c) (d)

Figure 4.6: Transformed Images obtained from (a)Lucas Kanade Optical flow, (b)Probabilistic Optical flow, (c)Demon's Algorithm and (d)Proposed Algorithm

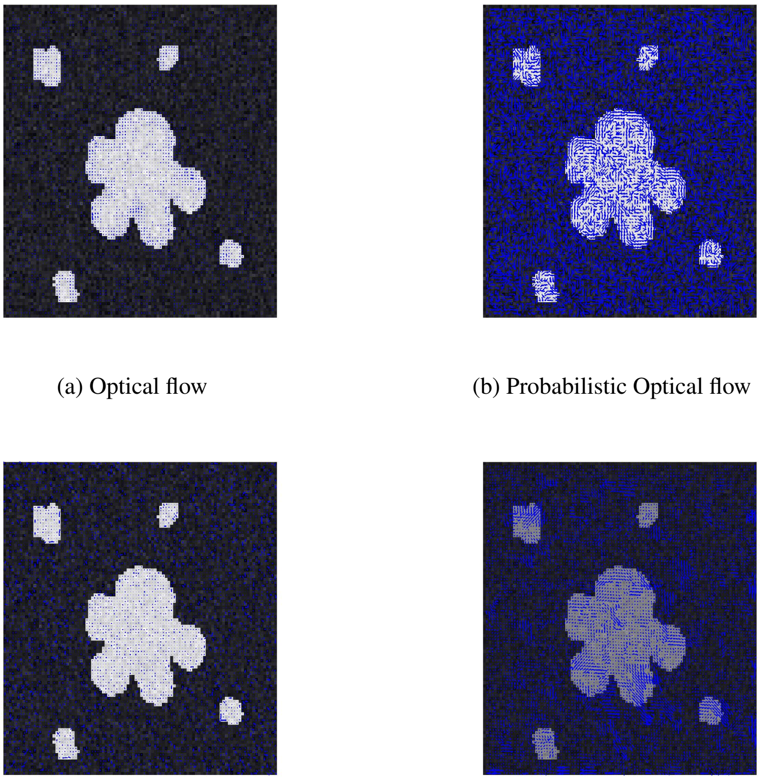

(a) Optical flow

(b) Probabilistic Optical flow

(c) Demons Algorithm

(d) Proposed Algorithm

Figure 4.7: Displacement field obtained using Optical flow and Image Registration algorithms discussed in this chapter

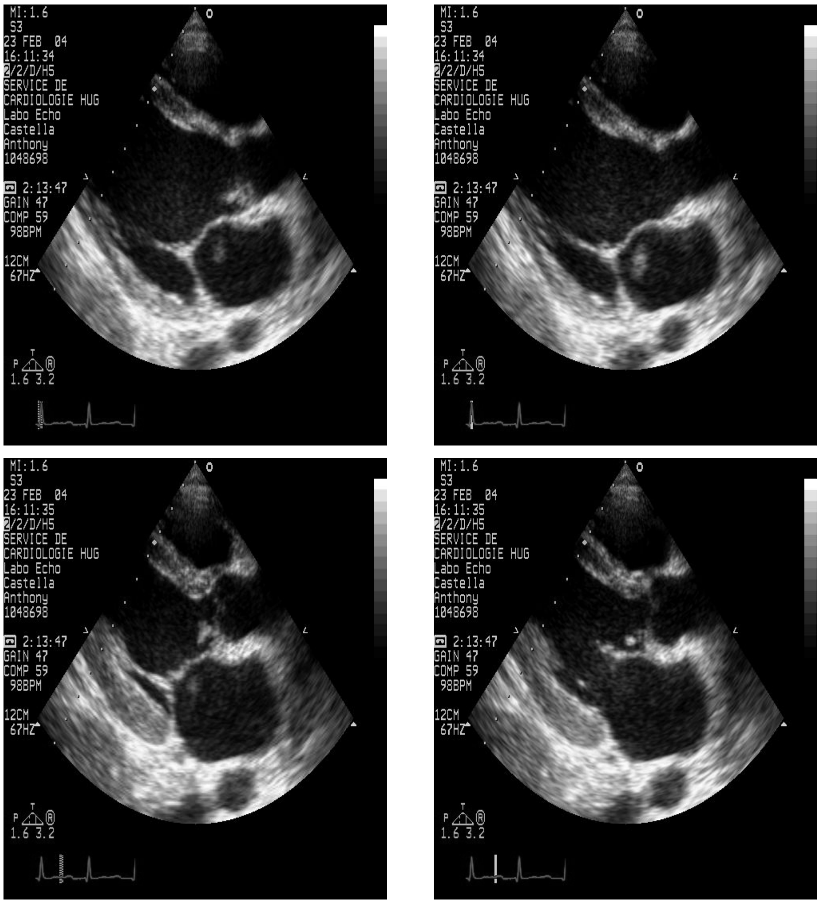

(a) Source Image (b) Moving Image

Figure 4.8: Echo-cardiographic images given as input to Optical flow and Image Registration algorithms

The results on original images are presented below. 4.8 shows two pairs of Source Image and Moving Image. The first row corresponds to the first pair of input images and the second row corresponds to the second pair of input images. The registered images are shown in 4.9, the first row consists of the registered images of first input image pair using Optical flow, Probabilistic Optical flow, Demon's Algorithm and Proposed Algorithm respectively. The images in second row correspond to the registered images of the second input image pair arranged in the same order as above. the Deformation field of the registered images of the second input image pair is presented in the 4.10. The results show that Demons algorithm performs better when compared to other algorithms.

The Quantitative results of the algorithms can be summarized as below. The table 4.1 consists the average of the SSD measure for each dataset individually.

The probabilistic optical flow performs better for both the synthetic datasets and demon's algorithm works better for the original algorithm. This is because we have pre-processed the images before the registration process. The performance of the algorithms is unexplainable because the Probabilistic frame-

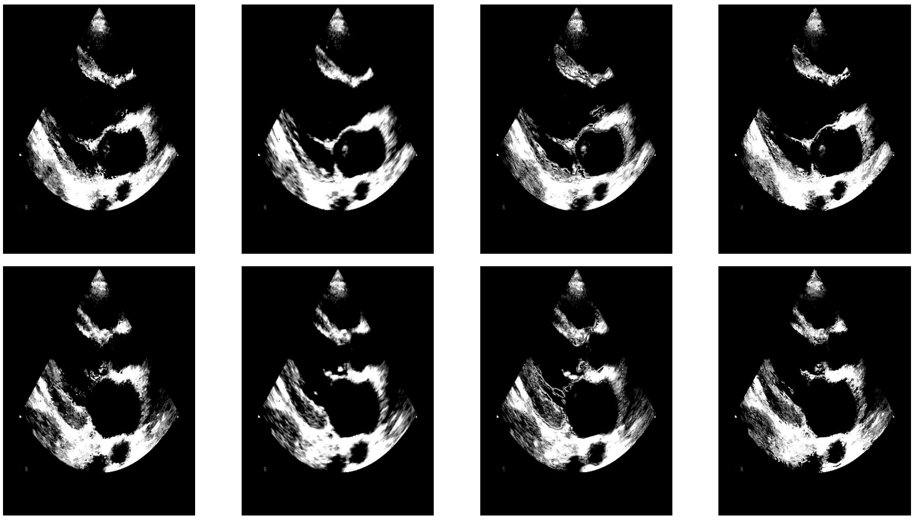

(a) (b) (c) (d)

Figure 4.9: Results obtained after transforming images using (a)Optical flow, (b)Probabilistic Optical Flow, (c)Demon's Algorithm and (d)Proposed Algorithm

Data	LK Optical Flow	VM Optical Flow	Demon's Algorithm	Proposed Algorithm
Synthetic Data 1	0.0036	**0.0010**	0.0038	0.0038
Synthetic Data 2	0.0136	**0.0110**	0.0185	0.0184
Original Images	0.0230	0.0218	**0.0201**	0.0215

Table 4.1: Average SSD obtained by four different algorithms (1) Lucas Kanade Optical flow, (2) Probabilistic Optical flow, (3) Demon's Algorithm and (4) Proposed Algorithm

work assumes that gaussian noise is added to the derivatives. It is not designed for the noisy images. But it still performs better in both the synthetic images. The proposed algorithm performs in the similar way as Demons algorithm for the synthetic datasets whereas for the original images it still is not a good algorithm to choose. Hence we need a better algorithm to handle the noise present in ultrasound images without the requirement of pre-processing step.

4.7 Summary

In this chapter an overview of possible variations that can be applied to demons algorithm to improve the performance of Demons algorithm is presented. A small variation of demons algorithm is designed based upon probabilistic framework of optical flow. The performance of this algorithm is compared with three different algorithms. However there is not much improvement in the algorithm. Hence there is a need for a better algorithm.

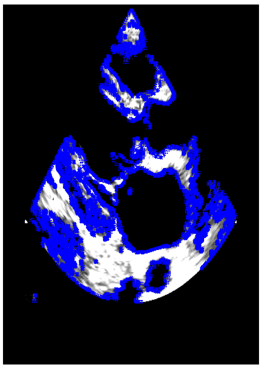

(a) Optical flow

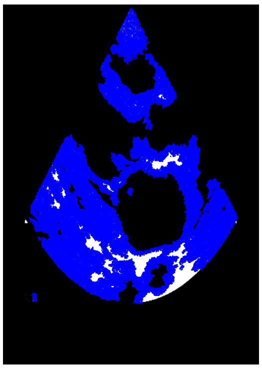

(b) Probabilistic Optical flow

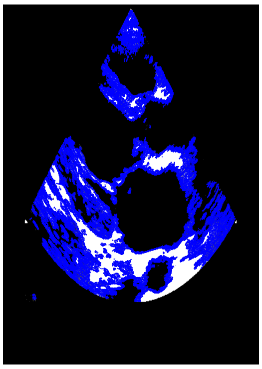

(c) Demon's Algorithm

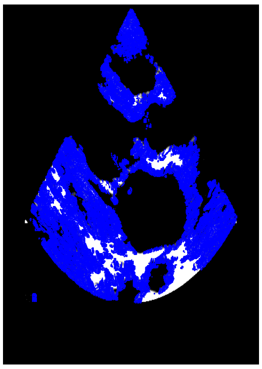

(d) Proposed Algorithm

Figure 4.10: Displacement field obtained using Optical flow and Image Registration algorithms

Chapter 5

Segmentation of Echo-cardiographic Images

5.1 Introduction

In this chapter we design a new representation of the image which is robust to noise. Since intensity cannot be directly used for the processing of the image because of the presence of high level of noise we need some information which describes the local-context of the image. Feature descriptors describe the local-context of the image when compared to intensity. We design a feature space representation of the image and test it with the other popular feature descriptors. The application that is used to showcase the use of this representation is image segmentation.

In image segmentation, the main aim is to be able to classify the pixels of the image into a set of non-overlapping regions. This can be done on the basis of similarity comparison of some aspect of the pixel. Hence, pixels which are similar are grouped together and those pixels which are dissimilar are divided into groups. The aspect used for comparison must be chosen meaningfully according to the image on which it is to be applied. In the case of natural images, where intensity sufficiently differentiates regions, intensity can be used for classification. But in the presence of noise intensity becomes inappropriate as it is inadequate. Using higher order information about the pixel might be a better solution.

As mentioned earlier, the main problems that make ultrasound image segmentation difficult are:

1. Speckle noise caused because back-scattering of the particles whose size is smaller than the wavelength of the projected waves [78] [5]. The noise depends upon the number of particles present in that particular tissue. This noise has been modeled using various distribution models like K-distribution, Nakagami etc. If the density of the scatterers is high then the noise is fully generated in tissue regions and half-generated in the blood regions.

2. During the acquisition of the image, the reflected waves are captured and then converted into image [5]. All the reflecting structures may not reflect the sound waves in the same direction due to difference in orientation hence the intensity of the waves is not same for similar reflecting structures which are oriented in different directions, hence there will be discontinuities in the edges in the ultrasound images.

3. There is a blurring effect along the direction perpendicular to that of the waves [5].

5.2 Related Work

Adapting intensity based techniques which are popular in general vision to ultrasound segmentation requires either de-noising via pre-processing or inclusion of the noise model in the algorithm. Pre-processing can remove extra information present in the image like speckle variations in different regions. Insertion of the noise models into the segmentation algorithms makes the design of the algorithm difficult and complex. A variety of geometrical or statistical approaches such as active contours [80] [17] [81] [82] [83] [84] [85] [63], Bayesian framework [86] [17], level-sets [87] [88] [89],neural network [90] etc have been proposed to address above mentioned challenges. In particular, level-set and active contour based techniques require a robust energy formulation to compensate noise factor, a challenging aspect in ultrasound images. However, high computation and time complexity make them inadequate for real-time application. For example, object tracking in a ultrasound image sequence a potential use case of the image segmentation.

5.3 Method

Our objective is to devise a solution that can handle noisy data naturally and yet produces good segmentation. Hence, we explore transforming the image into an appropriate feature space and segmenting via clustering in that space. The key here would be to identify the right feature space that is robust to noise. An existing attempt at clustering based approach for ultrasound segmentation is the spectral clustering technique [91] . In this, ultrasound images are first *pre-processed* using anisotropic filtering and then segmented using clustering. The proposed spectral clustering is based upon N-cut algorithm where the graph is built by similarity matrix between the pixels. This similarity matrix is built upon intensity. The eigen vectors obtained are used to get an embedding of pixels in low dimensional subspace and then a final partitioning is done based upon N-cut. In summary, to compensate noise factor they employ a pre-processing step and a strong clustering algorithm.

In this work, we argue that a similarity measure which is computed in an image descriptor space can provide better robustness to the noise compared to a measure defined solely on point intensity, as in . We propose a local point descriptor derived from the radon transform which is capable of capturing shape and intensity information reliably. To assess the strength of the proposed strategy, we do not handle noise explicitly by employing any pre-processing and uses a simple clustering scheme unlike spectral clustering used in [91]. Furthermore, a comparison is carried out against other popular feature descriptors like geometric blur, oriented histogram and DAISY to demonstrate applicability of the proposed descriptor. In the next section, we describe the proposed method in detail.

In order to segment such images, use of information about the local context of a pixel might be a good alternative. The local context represents the type of speckle noise present in the images and it is also robust to the blurring effect present in the image. We propose to derive a representation for the noisy image by locally transforming every pixel and constructing a feature descriptor for the pixel in this space.The choice of a particular feature descriptor depends upon the requirements like noise robustness, stability with respect to small distortions and invariance to geometric transformations.We choose the Radon transform and derive a descriptor in the Radon space.

The Radon Transform is an integral transform and some successful attempts have been made to derive representations from this transform to capture (largely binary or single grey scale) shape information [92]. However, it has not been applied in noisy grey scale images to derive a general local descriptor. The integral or projection operation underlying the transform should be useful in handling noise.

5.3.1 Feature Descriptor

The Radon transform T_{Rf} of a given continuous function f(x,y) is a projection along a line oriented at angle θ. It is given as

$$R^f\left(\rho,\theta\right) = \int_{-\infty}^{\infty}\int_{-\infty}^{\infty} f\left(x,y\right)\delta\left(x\cos\theta + y\sin\theta - \rho\right)\,dx\,dy, \tag{5.1}$$

where $\delta(.)$ is a Dirac delta-function. The range of the arguments are generally $\theta \in [0,\pi]$ and $\rho \in [-\infty,\infty]$. Note that the line is expressed in parametric form: $\rho = x\cos\theta + y\sin\theta$. The angle θ is also called the view angle.

In binary images, the Radon transform gives the length of intersection of the line with the object, which makes it a good representation of shape in binary images. In gray scale images, it is the line integral of the intensities. Thus, a rise in the intensity results in a high response. This helps it to differentiate between bright regions and dark regions which can be used in segmentation. The radon transform undergoes a shift in ρ under object translation and a shift in variable θ for object rotation.

Consider a feature-vector derived from the Radon transform by integrating the squared values of the Radon transform for every view θ as follows.

$$d(\theta) = \int_{\rho=-\infty}^{\rho=\infty} R^2\left(\rho,\theta\right)\,d\rho \tag{5.2}$$

The squaring operation boosts the high values of Radon transform. Since an object translation affects only the ρ variable, the feature descriptor $d(\theta)$ is unaffected. Object rotation by some angle θ_0 results in a translation of d by θ_0. Scaling affects only the magnitude of the feature-descriptor. Hence, this descriptor provides a good representation of the shape and context of a pixel.

Next we extend this idea to the discrete case. The line integral becomes a ray sum (projection). Let I[i,j] be the given image. Now consider a patch of size $n \times n$ around a pixel at location p.The Radon transform of this patch, denoted as $R[m,\alpha]$ is an array of size $(\sqrt{2})n \times K$ where K is the number of views. The descriptor d_p is constructed as follows. Next, the smoothed array is projected as follows

$$d_p[\alpha] = R[\alpha] = \sum_{m=1}^{m=(\sqrt{2})n} R^2[m,\alpha] \tag{5.3}$$

where d_p is a K-long feature vector.

An edge oriented at angle α_0 will yield a descriptor which has a maximum at α_0. Hence the descriptor forms a good representation of the shape or context present around the pixel. Since it is derived by summing the intensities along a particular direction, the descriptor is insensitive to zero mean noise. The descriptor is also resistant to blurring effect present in the image due to the projection operation (along m). Blurring spreads the intensity values but the information present in the actual image and the blurred image are same. Hence, there is no need for pre-processing the image.

In our implementation, each row of $R[m, \alpha]$ was smoothed with a 5-length kernel before deriving the descriptor. The aforementioned descriptor was computed for every pixel in the given image to obtain a representation of the image in a feature space.

5.3.2 Clustering

Since every pixel is associated with a feature vector, pixels belonging to similar regions (tissue type in ultrasound image) should cluster in the feature space. Thus, we classify these pixels based upon their corresponding feature vectors in the feature space. We use K-means clustering to achieve this classification. K-means clustering is one of the simplest and efficient ways of clustering when compared to other clustering methods like Agglomerative, Fuzzy K-Means and Mixture of Gaussians. In the present case, the target number of classes is found manually based on domain knowledge. Clustering results in each feature vector being assigned with a label. These labels are mapped back to the pixels of the image to get the segmented image.

5.4 Other descriptors of interest

Since the proposed scheme is one of clustering in a feature space, it is natural to ask if the choice of descriptor is correct. We consider other popular feature descriptors and wish to compare the segmentation performance across the descriptors. The descriptors that are considered are both gradient based and non-gradient based ones. In the former category are the histogram of oriented gradients used recently in non rigid registration [93] and the popular Daisy feature descriptor [94]. In the latter category is geometric blur [95] which is also good at representing shapes.

5.4.1 Geometric Blur

Geometric blur [95] is defined as the sum of blurred images in the polar coordinate space, where the blurring is done with a set of bounded transforms. Consequently, it is robust to geometric distortions. Details of the descriptor can be found in [95].

The method based upon this descriptor is referred as *GC*

It is defined as :

$$G_I(x) = \int_{T \epsilon \mathcal{T}} I(T(x))\, dT. \tag{5.4}$$

where geometric distortion T is contained in some set T of bounded transforms.

5.4.2 Histogram of Oriented Gradients

This descriptor is based on the assumption that the context of a pixel can be described by the distribution of gradients or edge directions. The descriptor is formed by computing the gradient orientation of the image and binning them. This descriptor [93] is similar to SIFT in a dense overlapping grid.

5.4.3 DAISY feature descriptor

This feature descriptor [94] is inspired from SIFT but is computationally faster. For a given image, to compute the DAISY descriptor, the gradient of the image in 8 different orientation is calculated. These gradient maps in 8 different orientations are then convolved with a Gaussian kernel having standard deviation Σ.

$$h_{\Sigma}(u,v) = [G_1^{\Sigma}(u,v), ..., G_8^{\Sigma}(u,v)]^T. \tag{5.5}$$

The full daisy descriptor at that point (u,v) is given as the concatenation of the h vector at different scales.

$$D(u_0,v_0) = \begin{bmatrix} h_{\Sigma_1}^T(u_0,v_0), \\ h_{\Sigma_1}^T(I_1(u_0,v_0,R_1)), ..., h_{\Sigma_1}^T(I_N(u_0,v_0,R_1)), \\ h_{\Sigma_1}^T(I_1(u_0,v_0,R_2)), ..., h_{\Sigma_1}^T(I_N(u_0,v_0,R_2)), \\ h_{\Sigma_1}^T(I_1(u_0,v_0,R_3)), ..., h_{\Sigma_1}^T(I_N(u_0,v_0,R_3)) \end{bmatrix}^T. \tag{5.6}$$

It is said to be robust to noise due to the Gaussian smoothing step.

5.5 Experiments

The proposed scheme for segmenting ultrasound images was implemented with the following settings. In the Radon transform computation of image patches, we chose m = 10 and K = 37. The number of clusters was chosen as per the test data. The segmentation performance was compared using our descriptor plus 3 other descriptors listed above. The performance was evaluated both qualitatively and quantitatively on two types of data described below.

5.5.1 Synthetic Data

A synthetic image was generated to have a dark circle on a white background with the intensity of the circle varying inversely according to a Gaussian function i.e., least at the center of the image and it increases as we move away from the center of the circle. Four such images are generated with decreasing radii. Since our main goal is to test the algorithm on noisy images, the images were corrupted with speckle noise generated using a Rayleigh distribution which is generally used to model speckle in ultrasound images. In [78], it is being proposed that the blood regions have less number of scatterers when compared to that of tissue regions, hence they low noise when compared to tissue region. Different noise statistics was used for the circle and its background to model the ultrasound image. Specifically, the noise level was set to be high for the background to model non-blood regions in an ultrasound and low noise noise level within the circle which models the blood region. Three different noise levels were studied. The segmentation algorithm was used to classify the pixels into 2 classes, namely, pixels belonging to the dark circle or the background.

5.5.2 Echo-cardiographic Data

Echo-cardiographic data is generally acquired in a video form. There are about 41 frames in each video. But the cycle of heart repeats after every 22 images. Hence, we evaluated the experiments only on 22 frames of echo-cardiographic data. These images were segmented to get blood and tissue regions.

5.5.3 Evaluation Measures

The obtained segmentation results were evaluated against human marked boundaries. We use following validation measures to report method's performance:

1. Rate of mis-classified pixels: The ratio of no. of mis-classified pixels to the total number of pixels present in target foreground region.

$$\mathrm{R}ate = \frac{\text{No. of mis-classified pixels}}{\text{Total No. of pixels present in the region}}. \tag{5.7}$$

2. Dice Coefficient: It gives the measure of overlap between two regions. If X is the segmented region and Y is the region present in ground truth then the measure is given as

$$Dice\ \ Coefficient = \frac{2 \times \mid X \cap Y \mid}{\mid X \mid + \mid Y \mid}. \tag{5.8}$$

5.6 Results

In our implementation, we use following parameter settings. In the Radon transform computation on image patches, we chose m = 10 and K = 37. The number of clusters chosen varied according to the underlying data. The descriptors other than ours, were computed using binaries provided by the respective authors.

First, we report experiment results for synthetic data. Figure 5.1 shows the segmentation results obtained on synthetic data corrupted with noise. The noise levels vary columnwise from low (top row) to high (bottom row). The results of clustering in different feature spaces are shown columnwise: From left to right these are for Histogram based (HC), Daisy based (DC), Geometric blur (GC) and FSC (ours) respectively. HC based clustering results are poor. The results of DC does not capture the desired circle boundary, it gives shifted boundaries but in high level noise it over segments in some cases. Comparatively, GC results are quite poor. The FSC results though a bit under-segmented are consistent across noise levels.

Table 5.1 shows the average rate of mis-classified pixels and the Dice coefficient obtained with different descriptors. The results of HC have been omitted as they were very poor. From this table, it can be seen that the overall performance of FSC is the best in terms of mis-classification and Dice coefficient. In the above evaluations, it can be seen that FSC performance is consistent across different noise

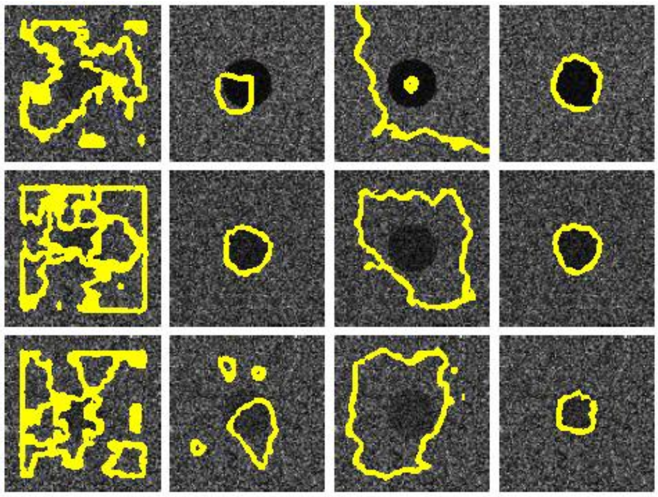

Figure 5.1: Results obtained on synthetic images corrupted with speckle noise by $a)$ first column: HC, $b)$ second column: DC, $c)$ third column: GC and $d)$ fourth column: FSC.

Feature	Rate of Misclassification	Dice Coefficient
DC	0.16	0.51
GC	0.62	0.27
FSC	**0.004**	**0.87**

Table 5.1: Average rate of misclassified pixels obtained by different descriptors

levels. This consistency makes it a good choice for echo-cardiographic segmentation. Next, we report experiments performed on the real echo-cardiographic data.

The segmentation results obtained on two echo-cardiographic image frames are shown in fig. 5.2. The red colour indicates region of interest (blood region) detected by proposed method (second column). In the last column, we show our results as follows: segmented blood region is indicated by white regions and the GT is visible as thin black contour and the non-blood tissue region is indicated by copying the original grey scale image. It can be seen that FSC is able to extract the regions of interest and distinguish it from the background regions quite successfully as over segmented regions are few.

Figure 5.3 shows the FSC results and results of other descriptors on the first image frame shown in the first row in fig. 5.2. It can be observed that FSC results are the most accurate. GC results appear to be the second best. However, the non-blood regions (not red) is very poorly handled in that it is inconsistent with the type of tissue characteristics seen in the original image. Inexplicably, DC failed completely.

Next, we quantitatively assess the performance of different methods. Only the GC and FSC have been considered for this purpose as the results of the rest of the methods are unacceptable. Table 5.2 shows the obtained values for FSC and GC, respectively for blood region. In Table 5.3, the mis-clasiffication rate for the tissue regions using FSC and GC are presented. It can be seen that on an average FSC gives low mis-classification rate (accurate segmentation), and high value of dice's coefficient (similarity with

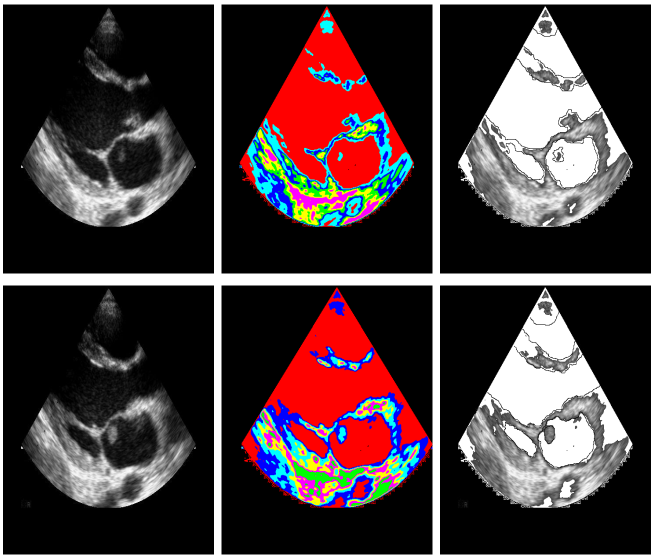

Figure 5.2: Two segmentation results on echocardiographic obtained by FSC. Each row shows a) original image b)segmented result and c) segmented result overlaid on ground truth (shown as thin contours).

Image	**Rate Of Misclassification**		**Dice Coefficient**	
	FSC	GC	FSC	GC
01	0.0065	0.35	0.95	0.78
05	0.0019	0.43	0.94	0.75
10	0	0.67	0.94	0.70
15	0.0032	0.51	0.89	0.66
20	0	0.48	0.86	0.68
Mean	**0.0023**	0.49	**0.91**	0.72

Table 5.2: Performance obtained on Echocardiographic Images for Blood Regions

the desired region) compared to the GC descriptor. A good performance on real echocardiographic data is mainly due to the robustness (in term of consistency) reported by the proposed descriptor on synthetic data. Hence from the qualitative and quantitative results, FSC shows consistency in all the evaluation measures.

5.7 Summary

In this chapter, a new segmentation algorithm has been presented for echo-cardiographic images based upon clustering of feature-space representation of the image. A feature descriptor is proposed for this purpose and computed for a patch around every pixel. This is derived from the Radon Transform. Test results from synthetic data demonstrate that the feature space clustering is most effective with the proposed descriptor as it provides robustness to different noise levels. This performance was also found

Image	**Rate Of Misclassification**		**Dice Coefficient**	
	FSC	GC	FSC	GC
01	0.011	0.59	0.75	0.40
05	0.004	0.58	0.74	0.41
10	0.008	0.54	0.73	0.42
15	0.017	0.55	0.74	0.42
20	0.014	0.51	0.72	0.43
Mean	**0.0108**	0.55	**0.74**	0.42

Table 5.3: Performance obtained on Echocardiographic Images for Tissue Regions

to hold for real images results. The obtained results on ultrasound images were assessed by a medical expert who found them to be qualitatively good. Any segmentation errors made by the algorithm were found to be more due to lack of inclusion of domain knowledge which a medical expert employs while marking. Example of this is in the top part of the image corresponding to myocardial muscle contour. Future efforts will be towards post processing of the segmentation results on the basis of such domain knowledge.

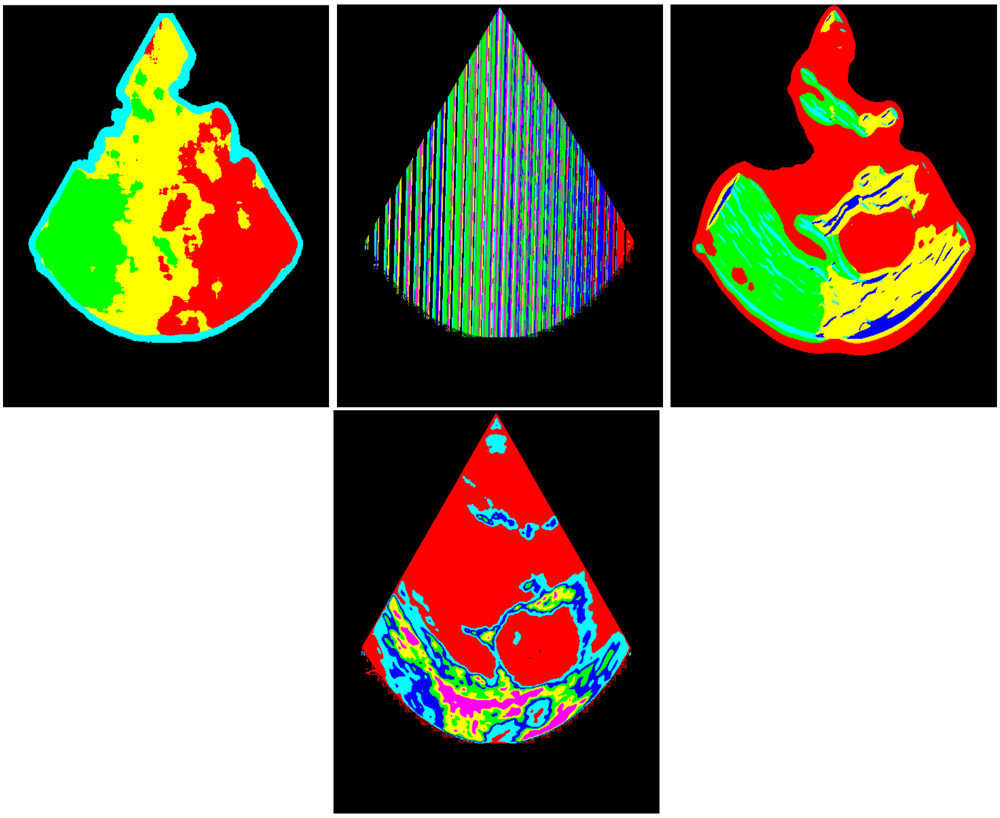

Figure 5.3: Segmented Echocardiographic images using HC,DC,GC and FSC

Chapter 6

Registration of Echo-cardiographic Images

6.1 Introduction

In this chapter we present a new algorithm for image registration of echo-cardiographic images. We specifically address the challenge presented by high-level of noise in such images. We do this by proposing a modification to Demon's algorithm. One common approach to Image registration process is to start with the matching of the objects or pixels with similar intensity in the images and then computing displacement between the matched points. A low-level feature like intensity is not appropriate to use in such images with high-level of noise. So, we need an alternative to intensity to compute the similarity between these images. The image registration algorithm proposed in this Chapter uses the Feature-space representation presented in Chapter 5.

Echo-cardiographic images undergo non-rigid motion due to the complex movement of the heart. Hence we require Non-rigid registration algorithm to align the echo-cardiographic images. Non-rigid Image Registration is more challenging when compared to rigid registration because it needs to model the transformation function such that the deformations in the images are handled. The transformation function is typically a displacement field, where the displacement is between frames. In the next section, we present an overview of exisiting algorithms for Non-rigid Image Registration and then describe the reason for choosing Demon's algorithm.

6.2 Related Work

There are a wide number of techniques [96, 97] proposed for non-rigid registration which are inspired from various fields like statistics, information theory, thermodynamics, optical flow, splines and block-matching. These techniques can be classified into a) feature-based techniques, in which prominent features in the images are matched based upon their geometric distance [98, 99]; b) intensity based techniques, in which similarity measure based upon the intensities is optimized and c) iconic feature-based registration, which falls in between feature-based and intensity-based techniques [100] which use a similarity measure to pair the features in the images without pre-segmentation.

Feature-based techniques are robust to noise but they completely rely on feature-extraction and there is an explicit step to compute the correspondences. Intensity based techniques are most widely used because of their simplicity but they easily get affected in the presence of noise. Iconic feature based methods being a hybrid method have the advantages of both the methods (a) and (b).

Demons algorithm proposed by Thirion [100] is one of the image registration algorithms in which components can be varied and it falls under all three categories. Though demons algorithm is most widely algorithm used for non-rigid registration of mono-modal images, it has few disadvantages which are mentioned in earlier chapters. The assumptions made in demons algorithm are (i) the displacement between the pixels is small, (ii) intensity remains constant over time and (iii) displacement field computation is based upon local measures. Due to these three assumptions the algorithm fails in the presence of large displacement, poor image contrast and illumination variation in images. Further it may not preserve the topology of the objects.

There are some algorithms which tried to improve the Demon's algorithm with suitable modifications. [100] proposed a normalization factor to the original Demon's algorithm to allow the length of the displacement vector to be adjusted adaptively.

[101] proposed a fast demons algorithm in which both static and moving images are symmetrically deformed towards one another. [11] criticized the inefficiency of using the gradient of the source image in the energy functional since smaller the gradient of the source image smaller the displacement field. This problem is solved by using the gradient of moving image is incorporated as a force term and the force is referred as active force. The demon's force in the original algorithm is referred as passive force. In another contribution [102], they combined both active forces and passive forces. The normalization factor adapted to the original demons algorithm was added to the algorithm in [11]. In [103], Diffeomorphic demons preserves topology and provides strong theoretical justification of demons algorithm due to the way in which its optimization is handled to register the multi-modal images. And others [103] have used other similarity measures in the form of intensity based similarity measure like mutual information and cross correlation.

[104] proposed a technique based upon the drawback of using optical flow in demons algorithm and proposed an extended method based upon Bayesian framework to make the algorithm work for high-texture regions. In the next section, we discuss the properties of the required algorithm and then later on discuss the proposed method in detail. We aim to replace the optical flow with a similar measure based upon the local-context of the image.

6.3 Properties of required algorithm

The algorithm which we design must be robust to noise. It implies that the matching of the objects or points in two images must depend upon some other criteria rather than intensity of the image. But in Demon's algorithm, the computation of displacement field depends upon the intensity of the moving image. This dependence on the intensity makes demon's algorithm very sensitive to noise, because when an image has high level of noise the intensity difference of same pixel can go to extremes irrespective of the local context. Hence there is a need to select only useful information from the intensities of the pixels like neighborhood information and just use that information instead of intensity for the computation of the displacement field.

For the registration algorithm to be robust to noise, it should have the following properties:

1. The displacement field computation should be robust to noise.
2. Pixels of Moving Image must be mapped to the similar regions in the Source Image.
3. The magnitude of the displacement field must be in such a way that it minimizes the distance between the Source and Moving Images.

6.4 Method

We adapt the demons algorithm such that it has the properties mentioned in Section 1.3. We go with the first variation of Demon's algorithm, since we are trying to minimize the distance between the images. Here, the displacement field is computed based upon local-context information of both the images.

As described in the Section 1.3, we need to have an information that is independent of noise, that represents the local context of the image and that can be easily used to compute the similarity of the images. The information which we choose is a Radon-Transform based representation of the image. This representation is achieved by mapping each pixel to the feature vector.

The distance measure which we use for registration is computed by using the steps:

1. At any given pixel, select a patch and compute radon transform of both Moving Image and Source Image to get Feature space representation of the images mentioned in Chapter 5.
2. Cluster the feature vectors at each pixel using K-means clustering
3. Compute the distance of each feature-vector from the centroid point of each cluster.

In Figure 6.7, we present the input image and its corresponding image which has the feature distance measure used for registration.

In Feature-space, this distance measure represents the variance of the feature vector in each cluster computed by k-means algorithm. In a ideal case we could have used information both mean and variance to represent feature-vector at each pixel position but to simplify the process we consider only variance at this point of time. Also, since underlying Brightness constraint in Demon's algorithm tries to localize the pixel position during the registration process, using the distance measure in the moving image and source image will map the regions with less displacement first(i.e., which belong to same cluster) and then proceed further. We use this distance measure in the energy functional for registering the images. The similarity measure computed between the Source Image and Moving image is the Sum of Squared difference of this distance measure for Moving Image and Source Image.

The energy functional is given as:

$$E = (D_S - D_M)^2 \tag{6.1}$$

where

$$D_S(x) = |\mathbf{Feature\_Vector(x) - Centroid\_k}| \tag{6.2}$$

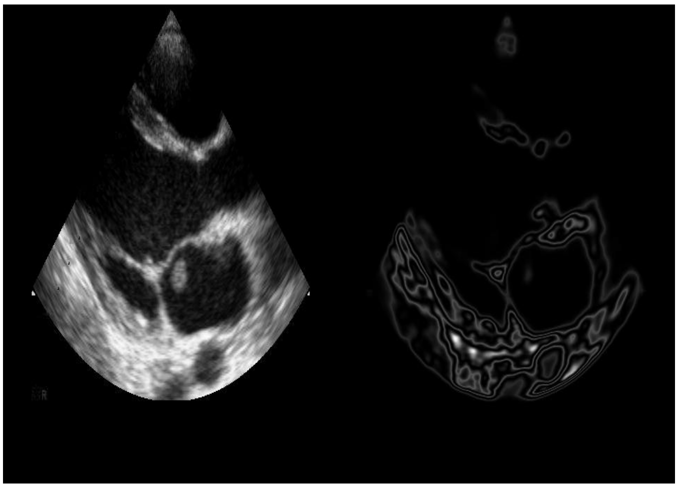

(a) Input Source Image (b) Feature Distance Map of the Input Source Image

Figure 6.1: Feature Distance Measure

x is the pixel location in D_S; D_S refers to the distance measure in Source Image S ; D_M refers to the distance measure in Source Image M ; $Feature\_Vector(x)$ is the Feature Vector computed at pixel location x ; $Centroid\_k$ is the Centroid of the class 'k' to which pixel x belongs in the image

The advantage of using this distance measure in energy functional is:

- **Representation of local context:** This information is computed from the feature-vectors is computed using Radon-Transform which gives a good local context information of the image. Hence it doesn't get affected with high level of speckle noise present in the images.
- **Localization:** The localization is handled internally by the brightness constraint assumption in Demon's algorithm. Similar regions are mapped to similar regions hence the distance measure in Moving Image will be mapped to similar distance measure in Source Image with minimal displacement. This case holds true for eacho-cardiographic images since the displacement is not that large.

Given Source Image and Moving Image, the steps carried out in our algorithm is: Compare Traditional Demons algorithm and this algorithm

1. Computation of the Distance measure at each pixel as mentioned above.
2. Starting Iteration for Registration with $i = 0$
3. Calculate the Energy function E between Source Image S and current Moving Image M_i
4. Compute Transformations T_{xi} and T_{yi} in the current iteration.

5. Apply the current transformation to modify the moving image i.e., $M_{i+1}(x) = M_i(T_i(x))$

6. Goto step 2. Repeat until the energy function has value less than threshold

At the end of this algorithm the moving image needs to be aligned to the source image, using the extracted motion field in Step 2. The similarity measure used in Demon's algorithm is based on intensity whereas in the proposed algorithm we use the similarity measure computed using local context information of the image. In the section below we present the results obtained using the proposed method.

6.5 Experiments

To evaluate our method, we have tested it on synthetic data, original data with synthetic deformations, and original data. The synthetic data is generated with linearly increasing noise level. We see that as the noise increases the demon's algorithm fails to compute the displacement field.

6.5.1 Data

Synthetic Data

The synthetic data used here is similar to that present in Chapter 5. It is generated to have a dark circle on a white background with the intensity of the circle varying inversely according to a Gaussian function i.e., least at the center of the image and it increases as we move away from the center of the circle. Four such images are generated with decreasing radii.

Since our main goal is to test the algorithm on noisy images, the images were corrupted with three types of noise: (1) Gaussian, (2) Speckle and (3) Salt and Pepper. Three different noise levels were studied. Speckle noise is generated using a Rayleigh distribution which is generally used to model speckle in ultrasound images [78].

Original Data

There are three sets of Echo-cardiographic image data-sets. One of them is obtained from internet database, the other two are from Care Hospitals and GE respectively. These data-sets are generally obtained as a video. We consider only the particular no. of frames for experiments in which constitute one full complete heart cycle.

We have conducted experiments with two types of data from the Original Images:

1. Original data with synthetic transformation

2. Original data with the frames extracted from the video

The first set of experiments are conducted to evaluate the algorithms using the evaluation measure computed from the Displacement field computed. We use synthetic transformations like swirl to represent the non-rigid deformation present in the images.

6.5.2 Comparison

The algorithms with which we compare are:

1. Traditional demons algorithm, the images are first pre-processed and then the registered(**DA**).
2. Proposed Algorithm based upon feature space(**FSA**).
3. Optical flow algorithm(**OF**).

6.6 Evaluation Measures

The evaluation measures used are:

6.6.1 SSD

Sum of squared difference between the Registered and the Target Image divided by total no. of pixels.

6.6.2 MDDF

This is computed only in the images which have the synthetic displacement field. It gives a difference in the magnitude of the displacement field overall the image. It is computed as:

$$MDDF = \frac{|ObtainedDF| - |GroundTruthDF|}{Totalno.ofpixels} \tag{6.3}$$

6.6.3 RDDF

This is computed only in the images which have synthetic displacement field. It gives a difference between the displacement fields in terms of the angle between them.

$$RDDF = \frac{\arccos{(ObtainedDF).(GroundTruthDF)/|ObtainedDF|.|GroundTruthDF|}}{Totalno.ofpixels} \tag{6.4}$$

6.7 Results

The results on synthetic data without noise is given below in Table 6.1. The SSD of the proposed algorithm and DA are similar and OF performs better than these two algorithms. But the Edge Overlap of the proposed algorithm is very low when compared to DA and OF.

The qualitative results are shown in the Figure 6.2. The synthetic images are arranged row-wise, first row corresponds to the images without noise, second row corresponds to the images with Gaussian noise, third row corresponds to the images with Speckle noise and the last row corresponds to the images with Salt and pepper noise. The results of the algorithms have been arranged column-wise, first column belongs to the Moving Image which is to be registered to Source Image, second column belongs

	FSA	*DA*	*OF*
No Noise	0.0031	0.0032	**0.0030**
Gaussian	0.070	0.067	**0.048**
Speckle	**0.15**	0.25	0.83
Salt and Pepper	**0.81**	0.90	1.5

Table 6.1: Average SSD for the synthetic images arranged by noise added to them

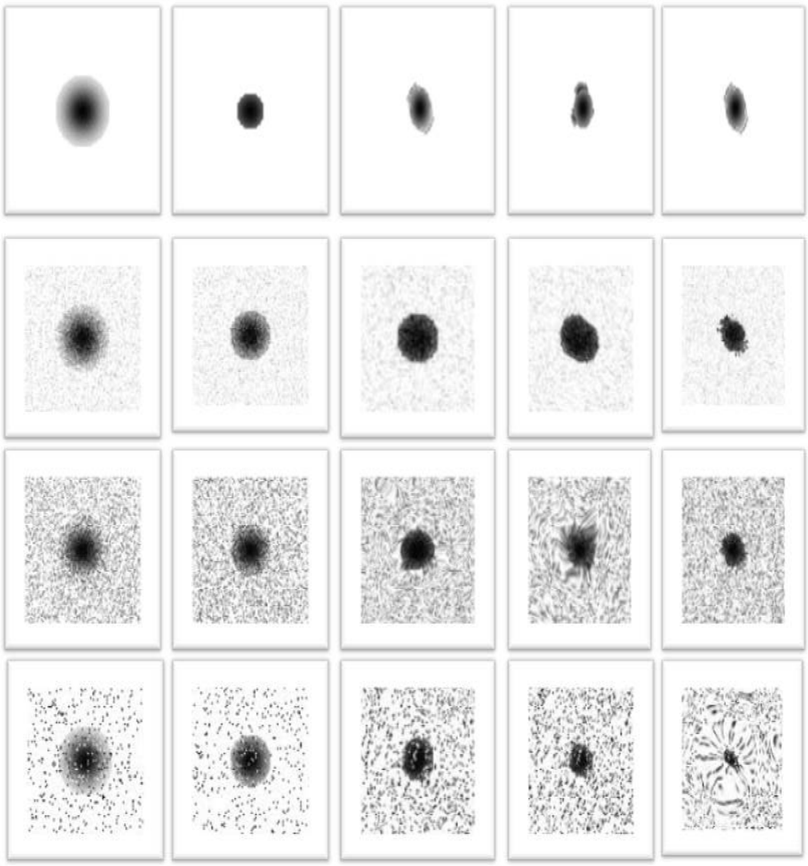

Figure 6.2: Row-wise top-bottom: (1) Synthetic Images without noise,(2) Synthetic Images with Gaussian noise, (3) Synthetic Images with Speckle noise and (4) Synthetic Images with Salt and Pepper noise and Column-wise left-right : (1) Moving Image, (2) Source Image,(3) Image Registered using FSA, (4) Image Registered using DA and (5) Image Registered using OF

	SSD	*MDDF*	*RDDF*
FSA	41.9	144.36	-38.36
DA	43.09	770.19	74.2
OF	67.7	197.14	-41.32

Table 6.2: Evaluation measures for Echo-cardiographic images

	FSA	*DA*	*OF*
Original data 1	24.8	23.6	21.1
Original data 2(GE)	17.5	20.42	18.71
Original data 3(Care)	22.31	24.9	22.32

Table 6.3: Evaluation measure SSD for Echo-cardiographic images

to Source Image, third column belongs to the Registered Image from FSA algorithm, fourth column belongs to the Registered Image obtained from DA(Demons algorithm) and fifth column belongs to the Registered Image obtained from OF(Optical flow). Based upon the results, we can see that Optical flow performs better in the images without noise and images with gaussian noise. But in the case of speckle noise, our proposed algorithm has performed better when compared to Demons algorithm and Optical Flow algorithm.

The results on original data with synthetic transformations is presented in the Table 6.2. As we can see from the table, proposed algorithm shows good results when compared to standard to Demon's algorithm. It performs equally well when compared to optical flow algorithm, in terms of Magnitude Difference of Displacement field(MDDF) and Angle difference of Displacement field.

The qualitative results for original data with synthetic transformations is presented below. In Figure 6.3, we present Moving Image and Source Image. In Figure 6.4, we present the obtained Registered Images from Proposed algorithm, Demons algorithm and Optical flow algorithm. We can see that the proposed algorithm performs equally well as Demons Algorithm. However, we find that the displacement field is smoothed out, this might be because of the reason that we consider the local context information of the image.

To compare the performance of the algorithms, we present the Moving Image and Source Image in Figure 6.5 and the obtained Registered Images in Figure 6.6. The results on three seperate datasets is given in Figure 6.7. The first column correspond to the Source/Target Image, the second column corresponds to the Moving Image, third column has registered images obtained using proposed algorithm and fourth column has the registered images obtained using Demons Algorithm respectively. These results show that the Demon's algorithm and Optical flow algorithms are sensitive to noise since the output image has a grainy look. However, the result of the proposed algorithm we get a smoothed registered image, this might be because we are using local context information.

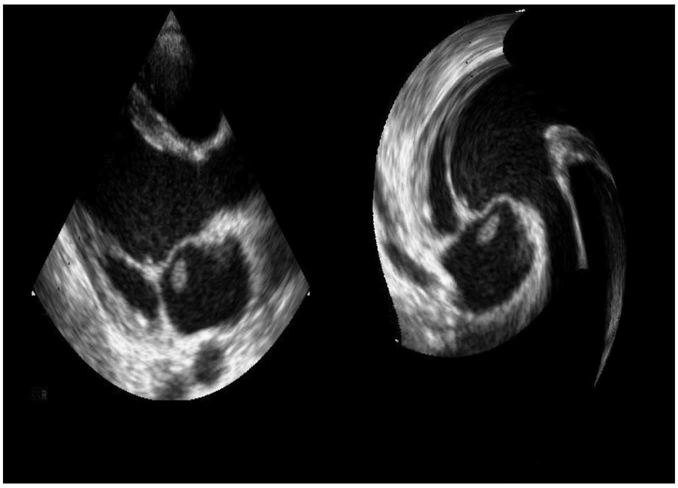

(a) Source Image (b) Moving Image

Figure 6.3: Test Images for Registration algorithm using Source Image and Moving Image created by applying a synthetic transformation to Source Image

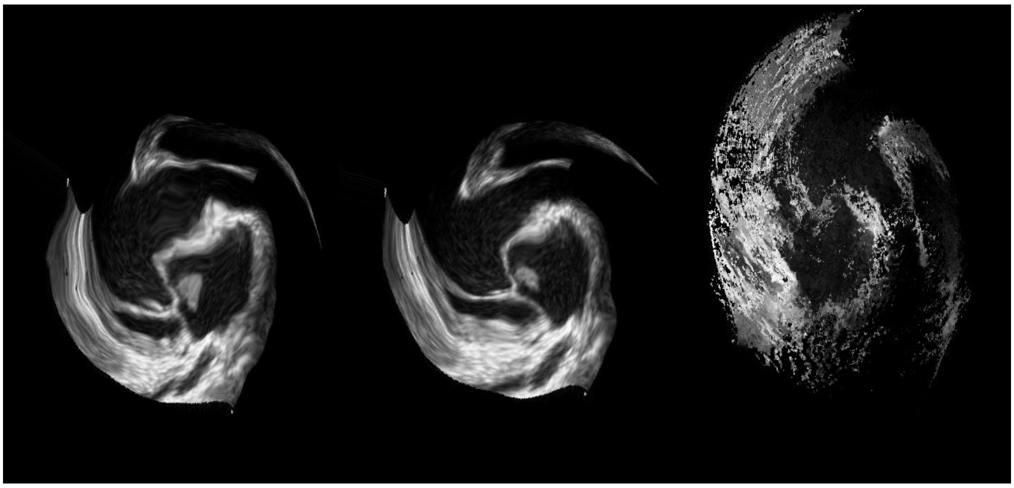

(a) (b) (c)

Figure 6.4: Transformed Images obtained using (a) Proposed Algorithm (FSA), (b) Demon's Algorithm (DA) and (c) Optical flow (OF)

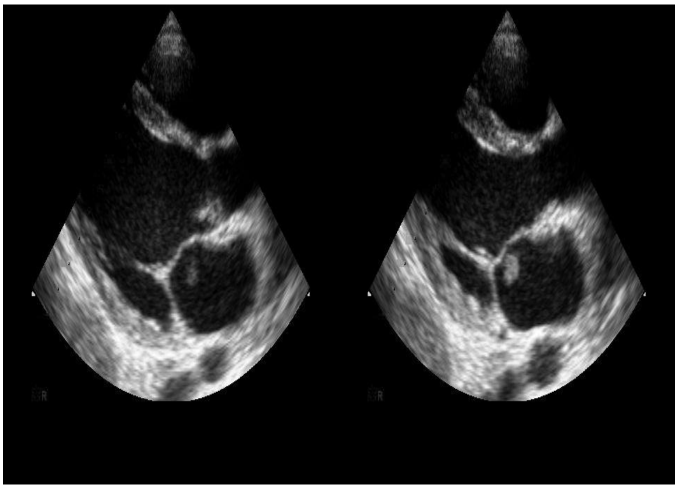

(a) Source Image (b) Moving Image

Figure 6.5: Input Images to validate the proposed algorithm for Image Registration

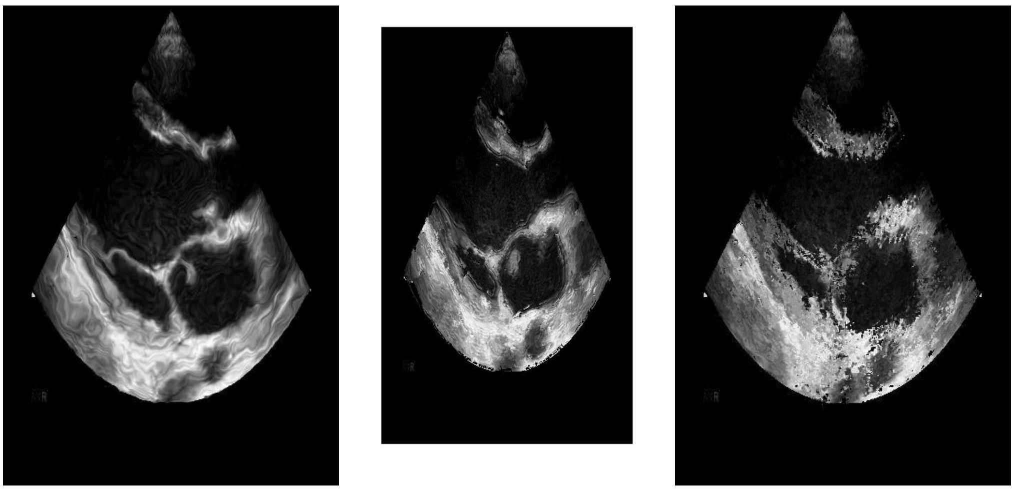

(a) (b) (c)

Figure 6.6: Transformed Images obtained using (a) Proposed Algorithm (FSA), (b) Demon's Algorithm (DA) and (c) Optical flow (OF)

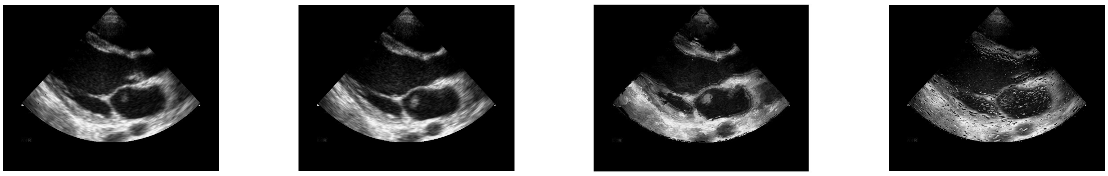

(a)

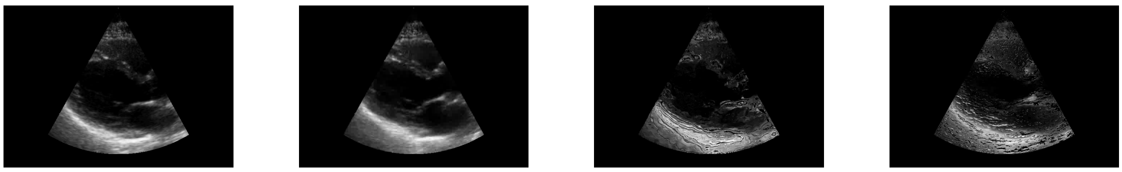

(b)

(c)

Figure 6.7: Results obtained after transforming images. (a) Target Image, (b) Moving Image, (c) Registered image using proposed method and (d) Registered image using Demons Algorithm

6.8 Conclusion

In this chapter, we present a new Image Registration Algorithm based upon Feature Space representation of the Image and is adapted from Demon's algorithm. The images are registered in a hierarchical way first class-label wise, then geometric position wise and at the end they are registered based upon the local context of the pixel. The algorithm is compared with traditional Demons algorithm and Optical flow. The performance of proposed algorithm is slightly improved when compared with Demons algorithm. However there is a requirement of a post-processing step in this algorithm to avoid the over-smoothing of the output image. But the post-processing of the images is not presented in this thesis. In future the performance of the algorithm can be improved by the inclusion of the post-processing of displacement field.

Chapter 7

Conclusions & Future work

7.1 Summary and Contributions

We have presented generalized methods for echo-cardiographic image analysis based upon feature descriptors. Our focus was on the use of feature descriptor which is robust to noise and which gives information about local context of the image to help traditional image processing algorithms like segmentation and registration. We have used Radon-transform based feature-descriptor in segmentation and registration of echo-cardiographic images. These methods can be generalised to other modalities like SAR where the noise is similar to speckle noise present in echo-cardiographic images.

Our objective was to design algorithms for echo-cardiographic image analysis which do not require any pre-processing. This has been achieved by creating the noise-robust representation of the image. The results have been shown on both synthetic and original images to access the performance of the algorithms as the noise level of present in the images increases. Proposed algorithm for Image Segmentation based upon feature-space representation has given good results for Radon-transform based feature vector when compared to other feature descriptors (DAISY, Geometric Blur and Histogram of Oriented Gradients). We can see that our method is a better noise-robust representation of an image when compared to other popular feature descriptors. Proposed Image Registration algorithm has given improvement in results when compared to existing Demon's Algorithm in presence of noise. However it is computationally expensive and it requires an additional step of post-processing. But the advantage of the proposed algorithm is that it performs better in presence of noise since it considers the local context of the image. It can be seen that our algorithm performs consistently over all the three datasets (1) Synthetic Images, (2) Original Images with synthetic transformation and (3) Original dataset of echo-cardiographic Images.

In summary we have proposed a feature-space representation for the image which can be used in the image analysis applications like segmentation and registration. We have shown the effectiveness of using feature-space representation and how this improves the performance of the algorithms. The application considered in thesis is motion analysis of echo-cariodgraphic images.

7.2 Future Scope

Though there are many algorithms for echo-cardiographic image analysis it is still an active area because of the high level of speckle noise present in it. More work can be done on experiments and application towards echo-cardiogaphic motion analysis. Possible extensions of the work are (i) Inclusion of complex learning algorithm in Image Segmentation, (ii) Post-processing in Image registration Algorithm , (iii) Trying to improvize on the speed of the algorithm by computing the feature descriptor at only required points rather than every pixel of the image and (iv) Comparision between normal and abnormal motion of the echo-cardiographic sequences. The algorithms presented in this thesis are not just limited to echo-cardiographic images, they can be used to other modalities like SAR, CT, MR etc and other applications too like object tracking etc.

Related Publications

- Vidhyadhari Gondle and Jayanthi Sivaswamy, “Echo-Cardiographic Image Segmentation : Via Feature Space Clustering“,in *Proceedings of the National Conference on Communications*, Bangalore, India, 2011.

Bibliography

[1] Q. Ciampi and B. Villari, "Role of echocardiography in diagnosis and risk stratification in heart failure with left ventricular systolic dysfunction," *Cardiovascular Ultrasound*, pp. 5–34, 2007.

[2] M. Foppa, B. Duncan, and L. Rohde, "Echocardiography-based left ventricular mass estimation. how should we define hypertrophy?," *Cardiovascular Ultrasound*, vol. 3, no. 1, p. 17, 2005.

[3] I. Mikic, S. Krucinski, and J. D. Thomas, "Segmentation and tracking in echocardiographic sequences: Active contours guided by optical flow estimates," *IEEE Trans. Med. Imaging*, vol. 17, no. 2, pp. 274–284, 1998.

[4] J. Melo, SalvadorA, B. Macchiavello, M. Andrade, J. Carvalho, H. Carvalho, D. Vasconcelos, P. Berger, A. Rocha, and F. Nascimento, "Semi-automatic algorithm for construction of the left ventricular area variation curve over a complete cardiac cycle," *BioMedical Engineering OnLine*, vol. 9, pp. 1–17, 2010.

[5] G. Jacob, J. A. Noble, C. P. Behrenbruch, A. D. Kelion, and A. P. Banning, "A shape-space based approach to tracking myocardial borders and quantifying regional left ventricular function applied in echocardiography," *IEEE Trans. Med. Imaging*, vol. 21, no. 3, pp. 226–238, 2002.

[6] G. Mailloux, F. Langlois, P. Simard, and M. Bertrand, "Restoration of the velocity field of the heart from two-dimensional echocardiograms," *Medical Imaging, IEEE Transactions on*, vol. 8, no. 2, pp. 143 –153, 1989.

[7] Y. Chunke, K. Terada, and S. Oe, "Motion analysis of echocardiograph using optical flow method," in *Systems, Man, and Cybernetics, 1996., IEEE International Conference on*, vol. 1, pp. 672 –677, 1996.

[8] M. J. Ledesma-Carbayo, J. Kybic, M. Desco, A. Santos, and M. Unser, "Cardiac motion analysis from ultrasound sequences using non-rigid registration," in *MICCAI*, pp. 889–896, 2001.

[9] V. Behar, D. Adam, P. Lysyansky, and Z. Friedman, "Improving motion estimation by accounting for local image distortion," *Ultrasonics*, vol. 43, no. 1, pp. 57–65, 2004.

[10] M. J. Ledesma-Carbayo, J. Kybic, M. Desco, A. Santos, M. Sühling, P. R. Hunziker, and M. Unser, "Spatio-temporal nonrigid registration for ultrasound cardiac motion estimation," *IEEE Trans. Med. Imaging*, vol. 24, no. 9, pp. 1113–1126, 2005.

[11] F. Wang, D. Beymer, and T. F. Syeda-Mahmood, “Spatio-temporal motion estimation for disease discrimination in cardiac echo videos,” pp. 121–124, 2008.

[12] J. Meunier, “Tissue motion assessment from 3d echographic speckle tracking,” *Physics in Medicine and Biology*, vol. 43, no. 5, p. 1241, 1998.

[13] D. Boukerroui, J. A. Noble, and M. Brady, “Velocity estimation in ultrasound images: A block matching approach,” in *IPMI*, pp. 586–598, 2003.

[14] E. R. K. K. J. C. R. J. O. M. Chen X, Xie H, “3-d correlation-based speckle tracking.,” *Ultrasound Imaging*, pp. 21–36, 2005.

[15] B. H. Amundsen, T. Helle-Valle, T. Edvardsen, H. Torp, J. Crosby, E. Lyseggen, A. Stylen, H. Ihlen, J. A. Lima, O. A. Smiseth, and S. A. Slrdahl, “Noninvasive myocardial strain measurement by speckle tracking echocardiographyvalidation against sonomicrometry and tagged magnetic resonance imaging,” *Journal of the American College of Cardiology*, vol. 47, no. 4, pp. 789–793, 2006.

[16] T. F. Syeda-Mahmood, F. Wang, D. Beymer, M. London, and R. Reddy, “Characterizing spatio-temporal patterns for disease discrimination in cardiac echo videos,” in *MICCAI (1)*, pp. 261–269, 2007.

[17] M. Mignotte, J. Meunier, and J.-C. Tardif, “Endocardial boundary e timation and tracking in echocardiographic images using deformable template and markov random fields,” *Pattern Anal. Appl.*, vol. 4, no. 4, pp. 256–271, 2001.

[18] H. S. Michal Lewandowski and I. Kowalik, “Searching for the optimal strategy for the diagnosis of stable coronary artery disease.cost-effectiveness of the new algorithm,” *Cardiology Journal*, vol. 14, no. 6, pp. 544–551, 2007.

[19] L. G. Brown, “A survey of image registration techniques,” *ACM Computing Surveys*, vol. 24, pp. 325–376, dec 1992.

[20] J.-P. Thirion, “Image matching as a diffusion process: an analogy with maxwell’s demons,” *Medical Image Analysis*, vol. 2, no. 3, pp. 243–260, 1998.

[21] B. K. Horn and B. G. Schunck, “Determining optical flow,” 1980.

[22] B. D. Lucas and T. Kanade, “An iterative image registration technique with an application to stereo vision,” in *Proceedings of the 7th international joint conference on Artificial intelligence - Volume 2*, IJCAI’81, (San Francisco, CA, USA), pp. 674–679, Morgan Kaufmann Publishers Inc., 1981.

[23] P. Baraldi, A. Sarti, C. Lamberti, A. Prandini, and F. Sgallari, “Evaluation of differential optical flow techniques on synthesized echo images,” *Biomedical Engineering, IEEE Transactions on*, vol. 43, no. 3, pp. 259 –272, 1996.

[24] P. T.Loupas, W.N.McDicken, “Adaptive weighted median filter for speckle suppression in medical ultrasonic images,” *Circuits and Systems, IEEE Transactions on*, vol. 16, no. 1, pp. 129 –135, 1989.

[25] S. Loncaric and T. Macan, “Point constrained optical flow for lv motion detection,” 2000.

[26] T. Macan and S. Loncaric, “3-d cardiac motion estimation by point-constrained optical flow algorithm,” 2001.

[27] Q. Duan, E. D. Angelini, S. L. Herz, O. Gérard, P. Allain, C. M. Ingrassia, K. D. Costa, J. W. Holmes, S. Homma, and A. Laine, “Tracking of lv endocardial surface on real-time three-dimensional ultrasound with optical flow,” in *FIMH*, pp. 434–445, 2005.

[28] I. Mikic, S. Krucinski, and J. D. Thomas, “Segmentation and tracking in echocardiographic sequences: Active contours guided by optical flow estimates,” *IEEE Trans. Med. Imaging*, vol. 17, no. 2, pp. 274–284, 1998.

[29] F. Veronesi, C. Corsi, E. G. Caiani, A. Sarti, and C. Lamberti, “Tracking of left ventricular long axis from real-time three-dimensional echocardiography using optical flow techniques,” *IEEE Transactions on Information Technology in Biomedicine*, vol. 10, no. 1, pp. 174–181, 2006.

[30] K. Y. E. Leung, M. van Stralen, A. Nemes, M. M. Voormolen, G. van Burken, M. L. Geleijnse, F. J. ten Cate, J. H. C. Reiber, N. de Jong, A. F. W. van der Steen, and J. G. Bosch, “Sparse registration for three-dimensional stress echocardiography,” *IEEE Trans. Med. Imaging*, vol. 27, no. 11, pp. 1568–1579, 2008.

[31] A. H. O. M. Adhi Harmoko Saputro, Mohd Marzuki Mustafa and I. F. M. Noh, “Motion estimation along the myocardial boundary using boundary extraction and optical flow,” in *World Congress on Engineering*, vol. 1, 2010.

[32] Z. R. Hussein, R. W. O. K. Rahmat, L. N. Abdullah, M. I. Saripan, and D. M. Zamrin, “Quantitative detection of left ventricular wall motion abnormality by two-dimensional echocardiography,” *Computer and Information Science*, vol. 3, no. 2, pp. 79–85, 2010.

[33] S. Riyadi, M. M. Mustafa, A. Hussain, O. Maskon, and I. F. M. Nor, “Enhanced optical flow field of left ventricular motion using quasi-gaussian dct filter,” *Software Tools and Algorithms for Biological Systems*, vol. 696, pp. 461–469, 2011.

[34] K. E. Leung, G. Mikhail, Danilouchkine, M. van Stralen, N. de Jong, A. F. van der Steen, and J. G. Bosch, “Left ventricular border tracking using cardiac motion models and optical flow,” vol. 37, pp. 605–616, 2011.

[35] F.-R. Sun, M.-Q. Zhang, X.-B. Jia, X.-J. Wang, G.-H. Yao, and Y. Zhang, “Region of interest tracking in real-time myocardial contrast echocardiography,” *J. Med. Syst.*, vol. 35, no. 2, pp. 163–167, 2011.

[36] M. Verhoek, M. Yaqub, J. McManigle, and J. Noble, "Learning optical flow propagation strategies using random forests for fast segmentation in dynamic 2d & 3d echocardiography," in *Machine Learning in Medical Imaging* (K. Suzuki, F. Wang, D. Shen, and P. Yan, eds.), vol. 7009 of *Lecture Notes in Computer Science*, pp. 75–82, Springer Berlin Heidelberg, 2011.

[37] v. R. O. Morsy AA, "Flash correlation: A new method for 3-d ultrasound tissue motion tracking and blood velocity estimation.," *IEEE Transactions on Ultrasonics, Ferroelectrics, and Frequency Control.*, vol. 46, no. 3, pp. 728–736, 1999.

[38] F. Contijoch, L. F. de Manuel, T. Ngo, J. Stearns, K. L. Grogan, M. Brady, P. Burlina, A. Santos, D. D. Yuh, D. A. Herzka, M. J. Ledesma-Carbayo, and E. R. McVeigh, "Increasing temporal resolution of 3d transesophageal ultrasound by rigid body registration of sequential, temporally offset sequences," in *ISBI*, pp. 328–331, 2010.

[39] Z. Zhang, D. Sahn, and X. Song, "Frame to Frame Diffeomorphic Motion Analysis from Echocardiographic Sequences," in *Proceedings of the Third International Workshop on Mathematical Foundations of Computational Anatomy - Geometrical and Statistical Methods for Modelling Biological Shape Variability*, (Toronto, Canada), pp. 15–24, 2011.

[40] K. McLeod, A. Prakosa, T. Mansi, M. Sermesant, and X. Pennec, "An incompressible log-domain demons algorithm for tracking heart tissue," in *Proceedings of the Second international conference on Statistical Atlases and Computational Models of the Heart: imaging and modelling challenges*, STACOM'11, pp. 55–67, 2012.

[41] K. Okamatsu, M. Takeuchi, H. Nakai, T. Nishikage, I. S. Salgo, S. Husson, Y. Otsuji, and R. M. Lang, "Effects of aging on left atrial function assessed by two-dimensional speckle tracking echocardiography," *Journal of the American Society of Echocardiography*, vol. 22, no. 1, pp. 70–75, 2009.

[42] A. Myronenko, X. B. Song, and D. J. Sahn, "Maximum likelihood motion estimation in 3d echocardiography through non-rigid registration in spherical coordinates," in *FIMH*, pp. 427–436, 2009.

[43] A. Gupta and K. ., "Statistical characterisation of speckle in clinical echocardiographic images with pearson family of distributions," *Defence Science Journal*, vol. 61, no. 5, 2011.

[44] A. Azar, H. Rivaz, and E. Boctor, "Speckle detection in ultrasonic images using unsupervised clustering techniques.," *Annual International Conference of the IEEE Engineering in Medicine and Biology Society.*

[45] C. B. Compas, B. A. Lin, S. Sampath, L. Huang, Q. Wei, A. J. Sinusas, and J. S. Duncan, "Comparing shape tracking, speckle tracking, and a combined method for deformation analysis in echocardiography," in *HISB'11*, pp. 120–125, 2011.

[46] N. T. Olsen, P. Sogaard, H. B. Larsson, J. P. Goetze, C. Jons, R. Mogelvang, O. W. Nielsen, and T. Fritz-Hansen, “Speckle-tracking echocardiography for predicting outcome in chronic aortic regurgitation during conservative management and after surgery,” *JACC: Cardiovascular Imaging*, vol. 4, no. 3, pp. 223–230, 2011.

[47] S. Finn, M. Glavin, and E. Jones, “Echocardiographic speckle reduction comparison,” *IEEE transactions on ultrasonics, ferroelectrics, and frequency control*, pp. 82–101.

[48] M. B. V. D. d. R. A. N. F. C. J. do Carmo Dos Reis M, Carvalho JL, “On the use of motion-based frame rejection in temporal averaging denoising for segmentation of echocardiographic image sequences.,” 2009.

[49] V. CHALANA, “A multiple active contour model for cardiac boundary detection on echocardiographic sequences,” *IEEE Trans. Medical Imaging*, vol. 15, no. 3, pp. 290–298, 1996.

[50] S. Martin, V. Daanen, O. Chavanon, and J. Troccaz, “Fast segmentation of the mitral valve leaflet in echocardiography,” in *Proceedings of the Second ECCV international conference on Computer Vision Approaches to Medical Image Analysis*, CVAMIA’06, (Berlin, Heidelberg), pp. 225–235, Springer-Verlag, 2006.

[51] P.-K. Chao, M.-H. Yao, H.-L. Chan, and C.-L. Wang, “Detecting endocardial boundary in echocardiogram by anisotropic filtering and entropy-weighted features,” in *5th European Conference of the International Federation for Medical and Biological Engineering* (k. Jobbgy, ed.), vol. 37 of *IFMBE Proceedings*, pp. 607–610, Springer Berlin Heidelberg, 2012.

[52] “A spatiotemporal statistical atlas of motion for the quantification of abnormal myocardial tissue velocities,” *Medical Image Analysis*, vol. 15, no. 3, pp. 316 – 328, 2011.

[53] P. Bansod, U. B. Desai, S. N. Merchant, and N. Burkule, “Segmentation of left ventricle in short-axis echocardiographic sequences by weighted radial edge filtering and adaptive recovery of dropout regions,” *Computer Methods in Biomechanics and Biomedical Engineering*, vol. 14, no. 7, pp. 603–613, 2011.

[54] A. Ciurte, N. Houhou, S. Nedevschi, A. Pica, F. L. Munier, J.-P. Thiran, X. Bresson, and M. B. Cuadra, “An efficient segmentation method for ultrasound images based on a semi-supervised approach and patch-based features,” in *ISBI*, pp. 969–972, 2011.

[55] A. Amichi and P. Laugier, “Quantitative texture analysis and transesophageal echocardiography to characterize the acute myocardial contusion.,” *Open Med Inform J.*, vol. 3, 2009.

[56] S. K. Zhou, J. Shao, B. Georgescu, and D. Comaniciu, “Pairwise active appearance model and its application to echocardiography tracking,” in *In Proc. MICCAI, volume I*, pp. 736–743, 2006.

[57] H. G. Bosch, S. C. Mitchell, B. P. F. Lelieveldt, F. Nijland, O. Kamp, M. Sonka, and J. H. C. Reiber, “Active appearance - motion models for fully automated endocardial contour detection in time sequences of echocardiograms,” in *CARS*, pp. 941–947, 2001.

[58] I. Dydenko, F. Jamal, O. Bernard, J. D'hooge, I. E. Magnin, and D. Friboulet, "A level set framework with a shape and motion prior for segmentation and region tracking in echocardiography," *Medical Image Analysis*, vol. 10, no. 2, pp. 162–177, 2006.

[59] T. Dietenbeck, M. Alessandrini, D. Barbosa, J. Dhooge, D. Friboulet, and O. Bernard, "Detection of the whole myocardium in 2d-echocardiography for multiple orientations using a geometrically constrained level-set," *Medical Image Analysis*, vol. 16, no. 2, pp. 386 – 401, 2012.

[60] A. Vard, A. Monadjemi, K. Jamshidi, and N. Movahhedinia, "Fast texture energy based image segmentation using directional walshhadamard transform and parametric active contour models," *Expert Systems with Applications*, vol. 38, no. 9, pp. 11722 – 11729, 2011.

[61] H. M., F. K., and B. S. . G. P., "Convex spatio-temporal segmentation of the endocardium in ultrasound data using distribution and shape priors.," in *Proc. The Eighth IEEE International Symposium on Biomedical*, pp. 626–629, 2011.

[62] B. Georgescu, X. S. Zhou, D. Comaniciu, and B. Rao, "Real-time multi-model tracking of myocardium in echocardiography using robust information fusion," *MICCAI*, pp. 777–785, 2004.

[63] X. Papademetris, A. J. Sinusas, D. P. Dione, and J. S. Duncan, "3d cardiac deformation from ultrasound images," in *MICCAI*, pp. 420–429, 1999.

[64] P. Viola, *Alignment by Maximization of Mutual Information*. PhD thesis, 1995.

[65] F. Maes, A. Collignon, D. V, G. Marchal, and P. Suetens, "Multimodality image registration by maximization of mutual information," *IEEE transactions on Medical Imaging*, vol. 16, pp. 187–198, 1997.

[66] M. Bro-nielsen and C. Gramkow, "Fast fluid registration of medical images," pp. 267–276, Springer-Verlag, 1996.

[67] e. a. Christensen G, Carlson B, "Image-based dose planning of intracavitary brachytherapy: registration of serial imaging studies using deformable anatomic templates," *Int J Radiat Oncol Biol Phys*, vol. 51, p. 22743, 2001.

[68] B. D. Lucas and T. Kanade, "An iterative image registration technique with an application to stereo vision," pp. 674–679, 1981.

[69] R. Szeliski and J. Coughlan, "Spline-based image registration," in *IN PROC. IEEE CONFERENCE ON COMPUTER VISION PATTERN RECOGNITION*, pp. 194–201, 1994.

[70] S. Fumihiko, "Image registration by block matching based on weighted gray-levels correlation," *Journal of the Institute of Image Electronics Engineers of Japan*, vol. 34, pp. 645–652, 2005.

[71] U. M. et al, "An enhanced block matching algorithm for fast elastic registration in adaptive radiotherapy," *Physics in Medicine and Biology*, vol. 51, 2006.

[72] P. J. Besl and N. D. McKay, “A method for registration of 3-d shapes,” *IEEE Trans. Pattern Anal. Mach. Intell.*, vol. 14, pp. 239–256, 1992.

[73] F. L. Bookstein and W. D. K. Green, “A feature space for derivatives of deformations,” in *Proceedings of the 13th International Conference on Information Processing in Medical Imaging*, IPMI ’93, pp. 1–16, 1993.

[74] R. F. Wagner, S. W. Smith, J. M. Sandrik, and H. Lopez, “Statistics of Speckle in Ultrasound B-Scans,” *Sonics and Ultrasonics, IEEE Transactions on*, vol. 30, no. 3, pp. 156–163, 1983.

[75] P. Mohana Shankar, “A general statistical model for ultrasonic backscattering from tissues,” *Ultrasonics, Ferroelectrics and Frequency Control, IEEE Transactions on*, vol. 47, no. 3, pp. 727 –736, 2000.

[76] P. Shankar, “A compound scattering pdf for the ultrasonic echo envelope and its relationship to k and nakagami distributions,” *Ultrasonics, Ferroelectrics and Frequency Control, IEEE Transactions on*, vol. 50, pp. 339–343, march 2003.

[77] I. Dydenko, D. Friboulet, J.-M. Gorce, J. D’hooge, B. Bijnens, and I. E. Magnin, “Towards ultrasound cardiac image segmentation based on the radiofrequency signal,” *Medical Image Analysis*, vol. 7, no. 3, pp. 353–367, 2003. Functional Imaging and Modeling of the Heart.

[78] O. Bernard, J. D’Hooge, and D. Friboulet, “Statistical modeling of the radio-frequency signal in echocardiographic images based on generalized gaussian distribution,” in *ISBI*, pp. 153–156, 2006.

[79] V. Govindu, “Revisiting the brightness constraint probabilistic formulation and algorithms,” vol. 3953, pp. 177–188, 2006.

[80] A. Mishra, P. K. Dutta, and M. K. Ghosh, “A ga based approach for boundary detection of left ventricle with echocardiographic image sequences,” *Image Vision Comput.*, vol. 21, no. 11, pp. 967–976, 2003.

[81] C. Xu and J. L. Prince, “Snakes, shapes, and gradient vector flow,” *IEEE Transactions on Image Processing*, vol. 7, no. 3, pp. 359–369, 1998.

[82] E. Brandt, L. Wigström, and B. Wranne, “Segmentation of echocardiographic image sequences using spatio-temporal information,” in *MICCAI*, pp. 410–419, 1999.

[83] A. A. Amini, T. E. Weymouth, and R. Jain, “Using dynamic programming for solving variational problems in vision,” *IEEE Trans. Pattern Anal. Mach. Intell.*, vol. 12, no. 9, pp. 855–867, 1990.

[84] J. G. Bosch, S. C. Mitchell, B. P. F. Lelieveldt, F. Nijland, O. Kamp, M. Sonka, and J. H. C. Reiber, “Automatic segmentation of echocardiographic sequences by active appearance motion models,” *IEEE Trans. Med. Imaging*, vol. 21, no. 11, pp. 1374–1383, 2002.

[85] M. Ma, M. van Stralen, J. H. C. Reiber, J. G. Bosch, and B. P. F. Lelieveldt, "Left ventricle segmentation from contrast enhanced fast rotating ultrasound images using three dimensional active shape models," in *FIMH*, pp. 295–302, 2009.

[86] D. Boukerroui, A. Baskurt, J. A. Noble, and O. Basset, "Segmentation of ultrasound images-multiresolution 2d and 3d algorithm based on global and local statistics," *Pattern Recognition Letters*, vol. 24, no. 4-5, pp. 779–790, 2003.

[87] J. Yan and T. Zhuang, "Applying improved fast marching method to endocardial boundary detection in echocardiographic images," *Pattern Recognition Letters*, vol. 24, no. 15, pp. 2777–2784, 2003.

[88] N. Lin, W. Yu, and J. S. Duncan, "Combinative multi-scale level set framework for echocardiographic image segmentation," in *MICCAI (1)*, pp. 682–689, 2002.

[89] Y. Chen, H. Tagare, S. R. Thiruvenkadam, F. Huang, D. C. Wilson, K. S. Gopinath, R. W. Briggs, and E. A. Geiser, "Using prior shapes in geometric active contours in a variational framework," *International Journal of Computer Vision*, vol. 50, no. 3, pp. 315–328, 2002.

[90] E. J. H. Wu, M. L. Andrade, D. E. Nicolosi, and S. C. Pontes, "Artificial neural network: border detection in echocardiography," 2008.

[91] N. Archip, R. Rohling, P. Cooperberg, H. Tahmasebpour, and S. K. Warfield, "Spectral clustering algorithms for ultrasound image segmentation," in *MICCAI (2)*, pp. 862–869, 2005.

[92] S. Tabbone, L. Wendling, and J.-P. Salmon, "A new shape descriptor defined on the radon transform," *Computer Vision and Image Understanding*, vol. 102, no. 1, pp. 42–51, 2006.

[93] S. Liao and A. C. S. Chung, "Non-rigid image registration with uniform spherical structure patterns," in *IPMI*, pp. 163–175, 2009.

[94] E. Tola, V. Lepetit, and P. Fua, "A fast local descriptor for dense matching," in *CVPR*, 2008.

[95] A. C. Berg and J. Malik, "Geometric blur for template matching," in *CVPR (1)*, pp. 607–614, 2001.

[96] H. Lester and S. R. Arridge, "A survey of hierarchical non-linear medical image registration," *Pattern Recognition*, vol. 32, no. 1, pp. 129–149, 1999.

[97] P. Cachier, E. Bardinet, D. Dormont, X. Pennec, and N. Ayache, "Iconic feature based nonrigid registration: the pasha algorithm," *Computer Vision and Image Understanding*, vol. 89, no. 2-3, pp. 272–298, 2003.

[98] T. Rohlfing, C. R. M. Jr., D. A. Bluemke, and M. A. Jacobs, "Volume-preserving non-rigid registration of mr breast images using free-form deformation with an incompressibility constraint," *IEEE Trans. Med. Imaging*, vol. 22, no. 6, pp. 730–741, 2003.

[99] R. Szeliski and J. Coughlan, “Spline-based image registration,” *International Journal of Computer Vision*, vol. 22, no. 3, pp. 199–218, 1997.

[100] X. Pennec, P. Cachier, and N. Ayache, “Understanding the demon’s algorithm: 3d non-rigid registration by gradient descent,” in *MICCAI*, pp. 597–605, 1999.

[101] D. Yang, H. Li, D. A. Low, J. O. Deasy, and I. E. Naqa, “A fast inverse consistent deformable image registration method based on symmetric optical flow computation,” *Physics in Medicine and Biology*, vol. 53, no. 21, p. 6143, 2008.

[102] P. Rogelj and S. Kovacic, “Symmetric image registration,” *Medical Image Analysis*, vol. 10, no. 3, pp. 484–493, 2006.

[103] T. Vercauteren, X. Pennec, A. Perchant, and N. Ayache, “Non-parametric diffeomorphic image registration with the demons algorithm,” in *MICCAI (2)*, pp. 319–326, 2007.

[104] D. Yang and H. Li, “A probabilistic demons algorithm for texture-rich image registration,” in *ICIP*, pp. 161–164, 2009.